# Construction, Optimization and Testing of a Coherent Anti-Stokes Raman Scattering Microscope

**THESIS**

Presented in Partial Fulfillment of the Requirements for the Degree Master of Science in the Graduate School of The Ohio State University

By

Minette C. Ocampo

Graduate Program in Chemistry

The Ohio State University

2011

Master's Examination. Committee:

Dr. Heather Allen, Advisor

Dr. Prabir Dutta

## ABSTRACT

Coherent anti-Stokes Raman scattering (CARS) microscopy is a nonlinear vibrational microscopy technique that generates an anti-Stokes signal that is used to detect the presence of chemical species based on their vibrational signature. This anti-Stokes signal is generated from the interaction of pump beam, Stokes beam and probe beam in a sample. CARS microscopy involves the combination of spectroscopy and microscopy that allows noninvasive characterization and imaging of chemical species without preparation or labeling. Three-dimensional sectioning with high sensitivity and resolution can be obtained from the contrast mechanism generated from the intrinsic molecular vibrational properties of the specimen.

This work presents the building of a broadband CARS microscope set-up in the Allen laboratory. It will discuss in detail the steps that were taken for the set-up and proper alignment of the system. A femtosecond Ti:Sapphire laser is used as the laser source and is divided into arms to form the pump and the Stokes beam. A photonic crystal fiber is used to generate the broad supercontinuum of light for the Stokes beam that will interact with the narrowband pump beam to generate a CARS signal at the sample focus. For the initial generation of a CARS signal, a forward CARS signal detection set-up was explored to produce a stronger CARS signal from a sample of liquid hexadecane. After ensuring correct alignment, that is, spatial and temporal overlap of the

two beams, a broad CARS signal was obtained for the $CH_2$ symmetric stretch. After generation of a forward CARS signal, the two beams are then sent to the microscope to generate an epi-CARS signal. At present, epi-detection is being set-up and optimized for the generation of an epi-CARS signal with a good spectral resolution and sensitivity.

Be still and know that I am God.

- *Psalms 46:10*

## ACKNOWLEDGMENTS

This long awaited thesis could not have been possible if it weren't for the help and encouragement from various people. First of all, I would like to thank my advisor, Dr. Heather Allen, for just simply believing in me and for providing the guidance, support and wisdom I need to finish this thesis and for always having time to bounce ideas off with. To Mr. John Carter of Newport Coporation, for always having time to answer my questions and for showing me patiently the techniques in building the instrument. To the members of the Allen group, in particular, Dr. Tang, Dr. Cheng, Dr. Sierra-Hernandez and Dr. Casillas-Ituarte, for their patience, encouragements and valuable insights that were instrumental to the success of this work.

I would also like to thank Mr. Hardy Castada for always extending an extra set of hands or eyes when needed and for the encouragement and friendship that has kept my sanity throughout this work. To my Filipino Christian Fellowship family and friends for always including me in their prayers. To my family, for trusting and believing in me even if the task seems daunting. And above all, to Almighty God, for his grace and faithfulness, and to whom I give back all glory, honor and praise.

## VITA

September, 1983.....Born—Angeles City, Philippines

2005.....B.S. Chemistry
University of the Philippines–Diliman

2005.....Chemist
NCA LABS-Philippines

2006-2008 .....Information Analyst
Information Analyst Corporation,
Makati City, Philippines

2008-2011.....Graduate Teaching Assistant
Department of Chemistry
The Ohio State University

2008-2011 ..... .....Graduate Research Associate
Department of Chemistry
The Ohio State University

## FIELDS OF STUDY

Major Field: Chemistry

## TABLE OF CONTENTS

## LIST OF TABLES

## LIST OF FIGURES

# CHAPTER 1

# INTRODUCTION

Vibrational spectroscopy is a powerful tool for the characterization of molecules based on the interactions of electromagnetic radiation with matter. When a molecule is placed in an electric field, a dipole moment is induced because the nuclei are attracted toward the negative pole of the field and the electrons are attracted to the positive pole of the field.[1] The molecules become polarized and the magnitude of the dipole moment induced is a measure of the polarizability of the molecular species.

Molecules have characteristic resonant frequencies which are independent of the applied electric field. When the frequency of the applied electric field is in resonant with the resonance frequency of the molecule, it absorbs a significant amount of energy.[2] Due to specific vibrational frequencies of molecules, vibrational spectroscopy, in general offers intrinsic chemical selectivity. The combination of vibrational spectroscopy and microscopy provides a noninvasive approach in probing specific molecular species. Microscopy techniques such as Infrared (IR) microscopy, fluorescence microscopy and Raman microscopy have found vast applications in varied materials and biological samples.

Although these vibrational microscopy techniques have seen rapid development over the past years, each method has its own disadvantages. In fluorescence microscopy, apart from the need to staining the sample, photobleaching of the fluorophore is another limitation. Photobleaching phenomenon occurs when photochemical side reactions modify the fluorophore and causes it not to absorb or fluoresce anymore.[3] IR microscopy, on the other hand, suffers from low sensitivity, low spatial resolution and water absorption of infrared light which makes this technique unsuitable for probing biological samples.[3]

Spontaneous Raman scattering microscopy avoids these problems and this technique has been extensively used in material and biological applications. The Raman process involves the interaction of energetic, high frequency visible or near-IR (NIR) light with the sample. The molecule is excited to a virtual state and then immediately returns to a lower state above the electronic ground state with the emission of a photon at a longer wavelength from the absorbed radiation (Figure 1.1A). The energy difference between the vibrational state and the ground state is defined as the Stokes shift. An anti-Stokes shift can also occur when the molecule is initially in the vibrational state (Figure 1.1B) and emits light at a shorter wavelength than the Stokes shift. The visible light excitation used in Raman microscopy provides a higher spatial resolution than that can be obtained from IR microscopy.[4] Raman microscopy also provides chemical selectivity and avoids the use of stains or labels for samples. Yet, despite these unique capabilities, its main limitation is in the application of the study of live cells. The Raman effect is extremely weak—this means longer acquisition times and high laser powers are needed

in visualizing samples. These factors can severely limit the application of this technique to the study of live cells or other biological specimens since it can easily cause thermal damage of the samples.

Stronger vibrational signals on the order of magnitude greater than spontaneous Raman scattering can be obtained with coherent anti-stokes Raman scattering (CARS). CARS is a four-wave mixing process wherein the pump, Stokes and probe beam interact with the sample to generate the anti-Stokes signal. Fluorescence background does not interfere with the signal detection since the signals are observed at higher energies relative to the excitation wavelengths.[3] During the last decade, with the rapid development of CARS microscopy, it has been employed in the study of lipids in model systems, measurement of molecular orientations, materials science and biomedical applications.

The formation of lipid microdomains or lipid rafts has been a hotly debated topic in biology. The main driving force on the formation of lipid rafts is the lipid-driven phase separation due to the presence of cholesterol, saturated and unsaturated lipids. Lipid rafts develop when saturated lipids form a liquid-ordered phase within a liquid-disordered sea of unsaturated lipids.[3] Laser scanning CARS has been used for the label free imaging of coexisting lipid domains in single bilayers. Li and co-workers demonstrated the ability of CARS microscopy in imaging lipid domains in single bilayers without the use of any labels.[5] Their work is based on the different lipid packing densities in the gel, liquid ordered and liquid-disordered phase which generates clear vibrational contrasts between coexisting domains. Orientation of water molecules

between closely packed lipid bilayers has also been investigated using the CARS technique. Cheng and co-workers showed that the water molecules close to the lipid bilayer surface are strongly ordered with their dipoles aligned against the bilayer dipole.[6]

CARS technique allows noninvasive characterization and imaging of chemical species and biological systems without preparation or labeling. Three-dimensional sectioning with high sensitivity and resolution can be obtained from the contrast mechanism generated from the intrinsic molecular vibrational properties of the specimen. The use of long-excitation wavelengths enables deep penetration for thick samples and reduces amount of light scattering in tissues.[7] Evans and co-workers demonstrated the imaging of a mouse skin tissue using a real-time video rate CARS imaging system.[8] They were able to visualize the abundant lipid structures up to 120 μm depth of the mouse ear skin. Similarly, Evans and co-workers used video-rate CARS to visualize brain structures in a section of the mouse brain.[9] Moreover, transdermal drug delivery was also studied using CARS.[7,10] In this work, the distribution and diffusion of 10% retinol solution when applied to a mouse ear skin was investigated and the drug is seen to concentrate between the corneocytes of the stratum corneum.

This thesis aims to describe in detail the construction and optimization of a broadband CARS microscopy instrument using the CARS kit acquired from Newport Corporation combined with an existing TE200S inverted Nikon microscope. This work will also detail the alignment of the photonic crystal fiber used to generate the supercontinuum needed for the Stokes beam. Generation and optimization of the CARS signal would then be demonstrated using dimethyl sulfoxide (DMSO) as the system of

study. Further recommendations will be outlined for the improvement of the instrument towards a more sensitive and optimized CARS system.

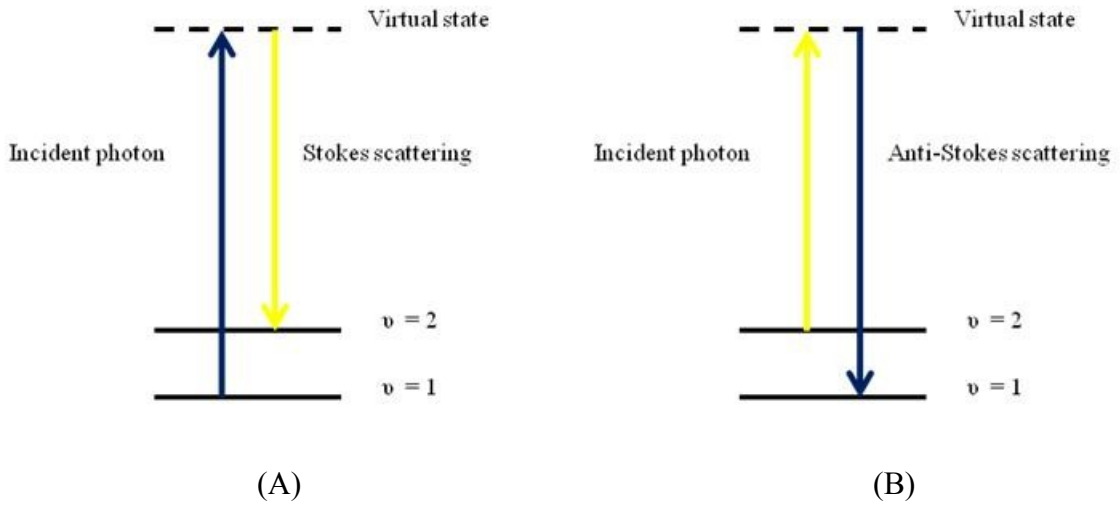


**Figure 1.1:** Energy level diagram for Raman scattering. (A) Stokes scattering (B) Anti-Stokes scattering.

# CHAPTER 2

# BACKGROUND THEORY OF CARS MICROSCOPY

## *2.1. Introduction*

In 1965, CARS as spectroscopic technique was first reported by P.D. Maker and R.W. Terhune at Ford Motor Company. Using a giant pulsed ruby laser, Maker and Terhune studied different nonlinear optical effects arising from an induced optical polarization third order in the electric field strength.[11] Their results show that two coherent light beams of frequency $\omega_1$ and $\omega_2$ can be used to drive a Raman vibrational mode at frequency $\omega_r = \omega_1 - \omega_2$ and produce a very strong signal.[11-12] Also, when the two beams are overlapped in space and time they observed a signal at $\omega+\omega_r$, which is the CARS signal.[13] At that time, they named this technique "three wave mixing experiments". Almost ten years later, Begley and co-workers named this optical process coherent anti-Stokes Raman spectroscopy. They evaluated the general use of this technique as a spectroscopic tool and showed that the signals obtained from this technique are about $10^5$ stronger than that from spontaneous Raman scattering.[14-15] Since then, CARS spectroscopy has become an important tool for the chemical analysis of gases, solids and condensed phases.

The first CARS microscope reported was in 1982 by Duncan and co-workers at the Naval Research Laboratory. In their work, they used two picosecond visible dye lasers as the light source with a noncollinear beam geometry and in the phase matching direction. They were able to obtain images of onion skin cells in $D_2O$ and other pure organic liquids.[4,16-17] However, the excitation geometry used in their work had some disadvantages. Among others, the spatial resolution along the axial dimension was low and the visible wavelengths resulted in a large nonresonant background and overwhelmed the vibrational contrast.[4,16]

Due to these technical difficulties encountered, there were relatively few developments until 1999 where Zumbusch and co-workers revived CARS microscopy.[16,18] They demonstrated vibrational imaging of chemical and biological samples with high spatial resolution, sensitivity and three dimensional sectioning capabilities by using near-infrared laser beams in a collinear geometry.[18] Most importantly, by using near-infrared pulses, the nonresonant background is much weaker than using visible excitation.[4] With these advancements in CARS, heightened interest resulted in more research groups and opened further developments in CARS microscopy. In 2001, Cheng and co-workers demonstrated the use of two picosecond Ti: Sapphire lasers to provide high spectral resolution.[19] In the same year, Volkmer and co-workers demonstrated epi-detection for the efficient rejection of the nonresonant background.[19-20] Other methods were also developed for the reduction of the nonresonant contribution and improvements in the image acquisition speed.

### *2.2 CARS Theory*

CARS is a more sensitive version of Raman spectroscopy wherein molecules are stimulated during their vibrational state to generate an anti-Stokes emission.[2] It is a nonlinear process in which three laser fields at the pump ($\omega_p$), Stokes ($\omega_s$) and probe ($\omega_{pr}$) frequencies interacts with the medium to generate a new field at the anti-Stokes frequency ($\omega_{as}$) (Equation 2-1):

$$\omega_{AS} = \omega_p - \omega_S + \omega_{pr} \tag{2-1}$$

The energy diagram of CARS is shown in Figure 2.1. Commonly, experiments use the same laser beam for the pump and the probe, simplifying the equation for the anti-Stokes frequency to:

$$\omega_{AS} = 2\omega_p - \omega_S \tag{2-2}$$

CARS signal can be significantly enhanced when the beat frequency ($\omega_p - \omega_s$) corresponds to a Raman active molecular vibration. By scanning the sample at a given beat frequency, the distribution of certain molecular species with a vibrational transition at this frequency can be mapped. Unlike Raman spectroscopy, where light scatters in all directions, CARS is a stimulated process, therefore the anti-Stokes signal recovers the momentum and energy of the incident photons and the anti-Stokes photon emits in the same direction as the incident photons in a coherent manner.[2,21] Since a higher frequency pump ($\omega_p$) and a lower frequency Stokes ($\omega_s$) is used, it follows from equations 2-1 and 2-2 that the anti-Stokes frequency ($\omega_{as}$) is higher than all excitation frequencies. This allows efficient separation of the signal by spectral filtering.[12] Also, autofluorescence and spontaneous Raman signals from the samples will be observed at

lower frequencies relative to the excitation frequency and will not interfere with the signal detection.

The induced dipoles from the CARS process are coherently superimposed and generates a third-order polarization, $P^{(3)}$, at the anti-Stokes frequency.[7] This induced polarization is determined by the field strength E of the excitation fields and the third-order nonlinear susceptibility of the material $\chi^{(3)}$:[3]

$$P^{(3)} = \chi^{(3)} E_p E_p E_S \tag{2-3}$$

$\chi^{(3)}$ is a fourth-rank tensor and is a complex quantity relating the complex amplitudes of the electric field and polarization.[22-23] Even when $\omega_p$-$\omega_s$ is detuned from a vibrational resonance, photons are still generated at $\omega_{as}$. Thus, there is a continuous nonresonant background level associated with CARS. It is then appropriate to decompose $\chi^{(3)}$ into its resonant and nonresonant components:[3]

$$\chi^{(3)} = \chi_R^{(3)} + \chi_{NR}^{(3)} \tag{2-4}$$

The intensity of the CARS signal is proportional to the square modulus of the induced polarization $P^{(3)}$:[3]

$$I_{CARS} \propto \left| P^{(3)} \right|^2 \tag{2-5}$$

$$I_{CARS} \propto \left( \chi_R^{(3)} + \chi_{NR}^{(3)} \right)^2 I_p^2 I_S \tag{2-6}$$

$I_p$ and $I_s$ are the intensities of the pump and Stokes beams respectively. From equation 2-6, it can be seen that the intensity of the CARS signal depends nonlinearly with the excitation intensity. The nonresonant part ($\chi^{(3)}{}_{NR}$) of the susceptibility has a purely

electronic origin and shows almost no frequency dependence in the absence of electronic resonances.[3,12] The resonant part ($\chi^{(3)}_R$) is given by:[5,16]

$$\chi_R^{(3)} = \frac{nA}{\delta - i\Gamma} \tag{2-7}$$

where $\delta = \Omega - (\omega_p - \omega_s)$, represents the detuning. $\Omega$ is the vibrational frequency, n is the number of oscillators with vibrational frequency $\Omega$, $\Gamma$ is the half-width at half maximum of the Raman line and A is a constant representing the oscillator strength. From equation 2-7, when $\omega_p - \omega_s$ is tuned to a molecular vibration $\Omega$, the intensity of the CARS signal is maximized. Also, the CARS signal varies with the square of the sample concentration. Since the intensity of the CARS signal is proportional to $(\chi^{(3)})^2$, this can be written as:

$$I_{CARS} \propto \left|\chi^{(3)}\right|^2 = \frac{n^2A^2}{\delta^2+\Gamma^2} + \chi_{NR} + \frac{2nA\chi_{NR}\delta}{\delta^2+\Gamma^2} \tag{2-8}$$

The first term contains the resonant contribution and the imaginary part of the vibrational response which also parallels the spontaneous Raman line.[7] The second term is the nonresonant background and is independent of the Raman shift. The third term is the cross-term and shows the mixing of the resonant and nonresonant contributions and contains the real part of the vibrational response.[5,7] Figure 2.2A shows the spectral response of each term and their individual contributions. The nonresonant part has a constant contribution while the imaginary part follows a Lorentzian profile and the real part shows a dispersive lineshape. This dispersive lineshape is from the interference of the nonresonant part to the resonant part and causes a redshift in the peak position and a dip at the higher energy side of the band.[7,12] This is seen in Figure 2.2B, which shows the typical shape of a CARS band. Note that the CARS band is slightly shifted to lower

energies with respect to $\omega_{vib}$ and a pronounced dip at the higher energy side of the band. This blue-end dip is not desirable since it gives negative contrast in CARS images.

Using classical or quantum mechanical calculations, it was is shown that $\chi^{(3)}$ can be expressed in terms of Raman scattering cross section. The resonant term of $\chi^{(3)}$ , $\chi_R^{(3)}$, is proportional to the amplitude strength, A, of the oscillator (Equation 2-7). The amplitude can be related to the differential Raman cross-section:[15]

$$A \propto \frac{\pi^2 c^4 n_P}{\hbar \omega_P \omega_S^3 n_S} \left(\frac{d\sigma}{d\Omega}\right) \tag{2-9}$$

where, $n_p$ and $n_S$ are the refractive index at the pump and Stokes frequency, respectively, and ($d\sigma/d\Omega$ ) is the differential Raman cross-section, wherein $\sigma$ is the Raman cross-section and $\Omega$ is the angle between the direction of observation and the electric vector of the plane polarized light.[11] The strength of the Raman signal is commonly expressed in terms of the differential scattering cross-section which gives the amount of scattered intensity for an incident frequency integrated over final frequency.[24] From this equation, it is shown that CARS is related to the normal Raman cross section and all molecular vibrations that are Raman active are also CARS active.

To directly compare the strength of the signal obtained from CARS over spontaneous Raman process, Tolles et al. at the Naval Research Laboratory derived the equation for the CARS signal power:[25]

$$P_{CARS} = \left(\frac{16\pi\lambda_S^4}{hc\lambda_P\lambda_{AS}}\right)^2 \left[\frac{N\Delta}{\Gamma}\left(\frac{d\sigma}{d\Omega}\right)\right]^2 P_P^2 P_S \tag{2-10}$$

For spontaneous Raman process, the power scattered is given by:[25]

$$P_{Raman} = NL\Omega \left(\frac{d\sigma}{d\Omega}\right) P_P \quad (2\text{-}11)$$

where, N is the number density, Γ is the full width at half maximum and L is the interaction length. Equations 2-10 and 2-11 indicate that the CARS signal has a cubic dependence on the laser power whereas normal Raman scattering has a linear dependence on the laser power. Tolles et al. showed that the CARS signal power obtained is orders of magnitude greater that the Raman signal power from a spontaneous Raman process. Using $H_2$ as an example, with $(d\sigma/d\Omega) \sim 2 \times 10^{-30}$ cm$^2$ and $\Gamma = 0.03$ cm$^{-1}$, L= 1 cm, the CARS signal average power calculated is ~ 3 X $10^{-4}$ W for a 10 pulse per second repetition rate using Equation 2-10.[25] Using the same incident power, a spontaneous Raman scattering process gives a ~ 2 X $10^{-8}$ W with Equation 2-11.[25] Their results showed that the CARS signal intensity is orders of magnitude greater than a spontaneous Raman signal.

Begley et al. using a similar method calculated the CARS conversion efficiency of the 992 cm$^{-1}$ Raman mode of benzene and obtained 2.0 x$10^{-3}$ CARS conversion efficiency which was greater than their spontaneous Raman calculated conversion efficiency of 6 x $10^{-8}$ using the same input power.[14] The calculated CARS value was tested by experiment, which revealed 0.5 W peak power at the detector for the benzene CARS signal for 1 kW peak input powers. This gave a conversion efficiency of 1.2x$10^{-3}$, close to the 2.0 x $10^{-3}$ calculated efficiency.[14]

### *2.3 CARS Microscopy*

The recent development of CARS microscopy has shown that the experimental requirements for CARS microscopy differ from that of CARS spectroscopy. The main difference is in the excitation geometry, where in CARS microscopy, the laser beams are tightly focused with a high numerical aperture objective lens.[3,16] Because of the coherent nature of the CARS process, a strong signal can be generated if the phases of the contributing electromagnetic waves are matched within the excitation volume.[12] The photons are emitted at an angle that conserves momentum and this is known as the phase matching condition. For the CARS process, the corresponding phase matching condition is given by :[3,12]

$$\left|\Delta k\right| l \ll \pi \tag{2-12}$$

where, l is the interaction length and Δk is the wave vector mismatch and gives the velocity difference of the three frequencies:

$$\Delta k = k_{AS} - (2k_p - k_S) \tag{2-13}$$

$k_{as}$, $k_p$, $k_s$ are wave vectors of the anti-Stokes, pump and Stokes fields, respectively. For CARS spectroscopy with a forward-detected geometry, the phase matching condition is commonly fulfilled by choosing an angle between the excitation beams.[12] To minimize the wave vector mismatch and maximize the interaction length, noncollinear beam geometries such as BOXCARS geometry were used.[16,26-27] Noncollinear beam geometries were also used for CARS microscopy experiments and allowed spatial separation of the excitation beams. This scheme in turn, leads to poor spatial resolution and the nonresonant background overwhelmed the vibrational contrast.[4,12,17] In 1999,

Zumbusch and co-workers demonstrated that CARS microscopy with collinear excitation geometry and under a tight focusing condition using a high numerical aperture objective lens led to a very strong CARS signal.[18] Under tight focusing conditions, phase matching is provided by the large cone of angles for the k-vectors of the exciting fields and small excitation volume.[12,28] Figure 2.3 shows the phase matching scheme commonly employed in CARS microscopy. Also, the phase matching condition in tightly focused beams is no longer sensitive to the Raman shift which allows recording of the CARS spectra in a collinear geometry for a broad spectral region without changing the alignment and provides good spatial resolution in the z-direction.[12,29-30] For this reason, CARS microscopy has an inherent 3D imaging capability without the need of confocal detection.

CARS signal can be obtained in the forward and the epi (backward) direction. The radiation pattern in CARS microscopy is dependent on both the size and shape of the scatterer and each vibrational oscillator can be considered as a Hertzian dipole at the anti-Stokes frequency[7,16,28] (Figure 2.4A). When the diameter of the scatterer is much smaller than the exciting wavelengths, CARS radiation propagates equally in the forward and backward direction as that from a single Hertzian dipole[7,16] (Figure 2.4B). As the sample thickness increases, the CARS signal almost exclusively propagates in the forward direction (Figure 2.4C) resulting in forward propagating CARS (F-CARS).

For bulk samples, constructive interference occurs in the forward direction and destructive interference in the backward direction leading to weak CARS signal in the epi-direction[7,16] (Figure 2.4D). For F-CARS, the CARS signal from the surrounding bulk

medium will also be collected in this direction and can severely limit the signal-to-background ratio and the imaging contrast. This is not the case for epi-directed CARS, which efficiently suppresses the background signal from the bulk medium.

Three mechanisms have been reported that gives rise to epi-directed CARS signal.[7,19] In the first mechanism, epi-CARS signal arises when the size of the sample is about one-third of the pump wavelength ($\lambda_p/3$) such as there is incomplete destructive interference that occurs in the backward direction. In the second mechanism, sharp discontinuities in the $\chi^{(3)}$ generates epi-CARS signal. The third mechanism involves redirecting of the forward CARS radiation towards the backward direction due to changes in the refractive index in the sample. This mechanism is found to be the primary contributor to epi-CARS signal from tissue samples.[7-8]

### *2.4 Multiplex CARS Microscopy*

Multiplex or broadband CARS microscopy allows higher selectivity by recording the spectra over larger frequency ranges. In single frequency CARS microscopy, a single point in the vibrational spectrum is addressed at a time by tuning the $\omega_p$-$\omega_s$ to match a Raman-active vibrational frequency which is time consuming. Broadband CARS microscopy allows fast data acquisition and recording of the entire CARS spectrum without tuning the Stokes frequency point by point and without changing alignment. In this excitation scheme, a narrow bandwidth laser serves as the pump/probe pulse and a broad bandwidth laser serves as the Stokes pulse. The interaction of both pulses allows

the probing of a wide range of vibrational levels.[3,29] Figure 2.5 shows the energy level diagram for multiplex CARS microscopy.

In a multiplex CARS experiment by Cheng and co-workers, a near IR laser system was employed consisting of a picosecond Ti:Sapphire laser for the pump/probe beam synchronized with a femtosecond Ti:Sapphire laser for the Stokes beam in a collinear geometry in the study of lipid vesicles.[29] The spectral profile of Ti:Sapphire lasers is more stable than that of dye lasers which are used in previous studies.[29,31-32] They also demonstrated that their multiplex CARS set-up allows high-speed spectral characterization with high spectral resolution of microscopic samples.[29] Moreover, Muller and co-workers have reported multiplex CARS imaging for the first time by fitting the multiplex CARS spectrum for each pixel of an image.[16,30] This also allows identification of two or more chemical species in one scan using their Raman band lines in the CARS spectral profile.[16,33]

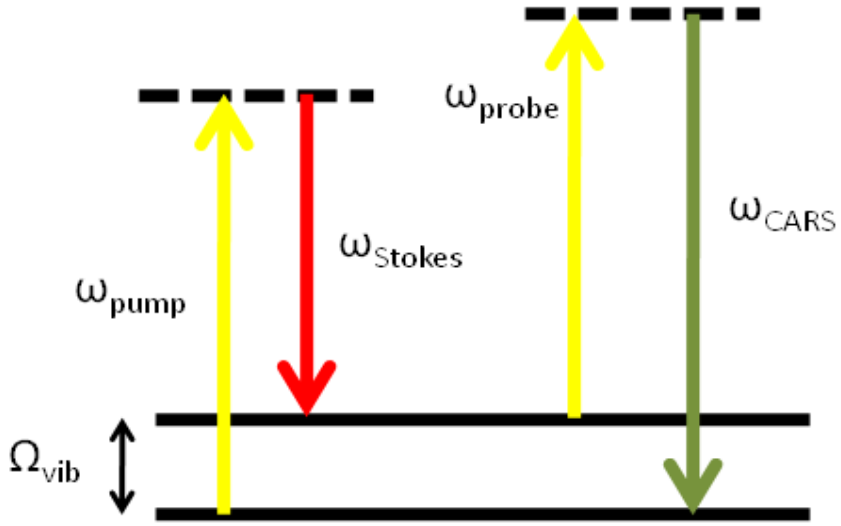


**Figure 2.1:** Jablonski diagram for the CARS process.

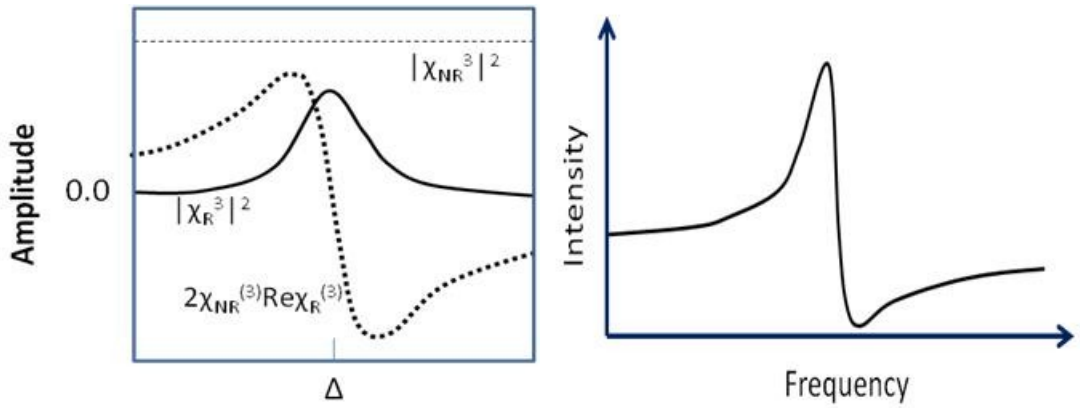


**Figure 2.2:** (A) Three components of the CARS signal plotted as a function of detuning. (B) Typical shape of a CARS band.

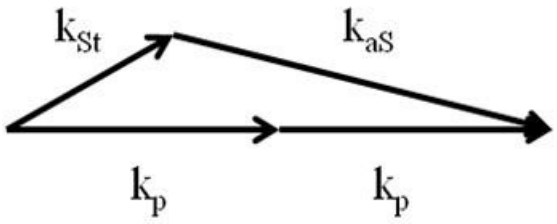


**Figure 2.3:** Phase matching condition for the CARS process.

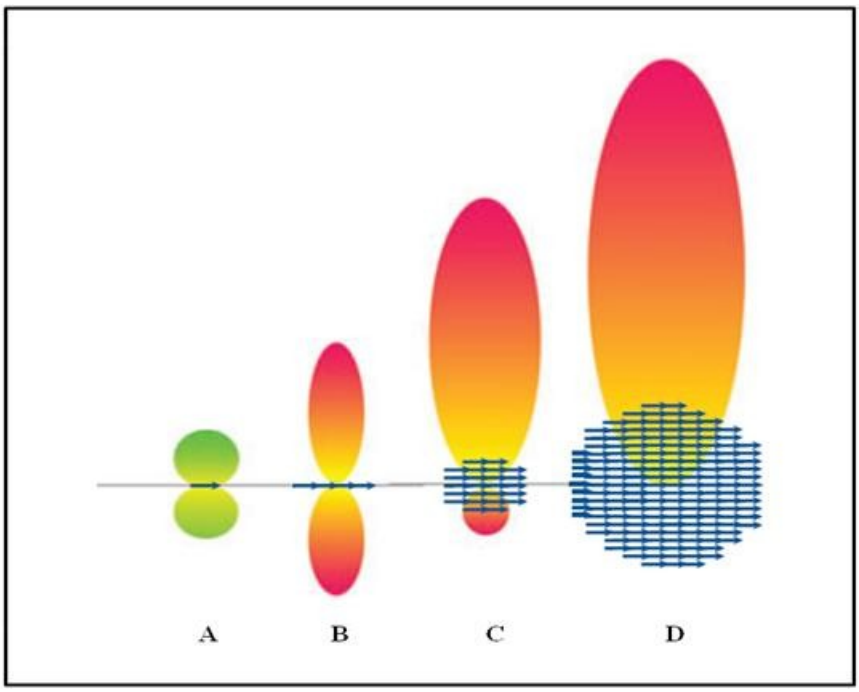


**Figure 2.4:** Effects of CARS signal buildup at the focal volume adapted from Evans et al (2008)[7]. (A) Radiation pattern of a single Hertzian dipole. (B) Plane of dipoles coherently add to generate forward and backward CARS signal. (C)Few induced dipoles add together to generate a strong forward CARS signal and a weak epi-CARS signal. (D) An ensemble of induced dipoles such that from a bulk sample, coherently interfere to generate only a strong forward CARS signal.

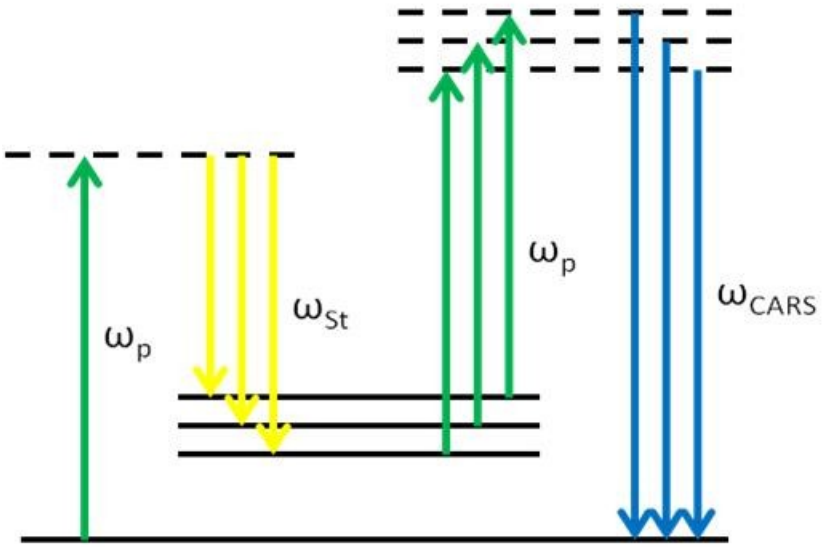


**Figure 2.5:** Energy level diagram for a multiplex CARS excitation scheme.

# CHAPTER 3

# EXPERIMENTAL SET-UP AND PROCEDURES

## *3.1 Introduction*

This chapter details the set-up and alignment of the CARS microscope. The broadband CARS microscope is based on the CARS microspectrometer set-up by Newport Corporation[34]. In this broadband approach, the pump pulse has a narrow bandwidth and the Stokes pulse is spectrally broad and in the femtosecond regime.[34] The bandwidth of the pump pulse defines the spectral resolution of the CARS spectrum. A supercontinuum light source generated by a photonic crystal fiber (PCF) is used as the Stokes pulse. The interaction of the narrow band pump and broadband Stokes excites multiple Raman transitions within the bandwidth of the Stoke pulse. These vibrationally excited states are probe with a third narrow bandwidth pulse, which is usually the same as the pump pulse. An anti-Stokes signal is then generated and in a single measurement the entire CARS spectrum can be obtained.

### *3.2 CARS Set-up*

The CARS set-up consists of five primary sections, namely: laser source, supercontinuum generation, microscope, detector and computer for data acquisition. The optics needed to build the set-up were obtained from the CARS kit of Newport Corporation. The remainder of this section will detail the optics and individual components used for the set-up. The block diagram of the CARS set-up is shown in Figure 3.1 and the actual microscope set-up is shown in Figure 3.2.

#### *3.2.1 The Laser Source*

The laser source used in this set-up is a near-IR (NIR) amplified mode-locked Ti:Sapphire laser (Tsunami, Spectra-Physics) with sub-50 femtosecond 782 nm pulses and a repetition rate of 82 MHz Using NIR laser sources has its advantages. NIR sources minimize two-photon interactions and therefore provide better signal-to-noise ratios.[7,16] They also minimize photo-damage of specimens and maximize penetration depth in tissue samples allowing for deep CARS imaging.[7] Since the signal in the CARS process has a quadratic dependence on the pump field intensity and a linear dependence on the Stokes field intensity[16], it is then preferred to use pulsed laser systems. Ti: Sapphire fs laser has the capability to provide intense laser pulses at a low average power that limits the damage to the sample.[2]

The measured power for the Ti:Sapphire laser output is about ~ 593 mW and a mirror (10D20ER.2, Newport Corp.) mounted on a kinematic mirror mount (SN100-F2K, Newport Corp.) is carefully placed after the output port of the Ti:Sapphire laser and is

set to 45° to bring the beam towards the CARS set-up in a straight path. The beam is then directed towards the periscope to stir the beam down and change the polarization from vertically to horizontally polarized light. The height of the beam is critical at this point since it has to match the height of the photonic crystal fiber (PCF) for the Stokes beam. The horizontally polarized beam is now reflected using a mirror (SN100-F2K, Newport Corp.) towards the Faraday optical isolator (ISO-05-800-BB-G, Newport Corp.). The Faraday isolator separates the laser from the rest of the set-up and prevents multiple back reflections from reaching and damaging the laser source. This optical isolator uses a Glan laser calcite type of polarizing material that requires horizontal polarization for the beam input.[34-35] The polarization state of the output beam from the Faraday isolator is vertically polarized and is then divided into two beams by a beamsplitter (10RQOOUB.2, Newport Corp.) forming the pump and Stokes beams.[34] The splitting ratio of the beamsplitter is 50/50 for vertically polarized light and at a 45° incident angle.

#### *3.2.1.1 Pump Beam*

Fifty percent of the 593 mW output power of the Faraday isolator is reflected to serve as the pump beam. The beam then passes through a variable attenuator which is based on a half-wave plate (10RP52-2, Newport Corp.) and a Glan laser polarizer (10GL08AR.16, Newport Corp.). These optics attenuate the linearly polarized laser beam in the wavelength range of 690 – 1040 nm.[36] The half wave plate is mounted on to a rotational stage (RSP-1T, Newport Corp.) which allows continuous rotation of the

beam's polarization.[36] When the half wave plate is combined with a Glan laser polarizer, they provide variable attenuation of the intensity of the laser.

After the beam passes through the attenuator, it is then mirror-directed towards the delay line for the pump beam. The beam passes through a 780 nm bandpass filter which narrows the spectrum of the beam to 3 nm centered at 780 nm. Figure 3.3 shows the spectrum before and after the beam passes through the bandpass filter. The pump beam recombines with the Stokes beam after reflecting from a 780 nm razor edge longpass filter (LP02-780RU-25, Semrock). The pump beam is then directed towards the beam steerer to get the desired height of the laser that matches the height of the entrance port of the microscope. A dichroic shortpass filter (785DRSP, Omega Optical) inside the filter wheel, located under the revolving nosepiece, reflects the pump beam towards the objective lens to focus beam on to the sample. Figure 3.4 shows the transmission spectrum for the dichroic shortpass filter. The filter reflects wavelengths longer than 785 nm and transmits wavelengths less than 785 nm.

#### *3.2.1.2 Stokes Beam*

The remaining 50% of the output power from the Tsunami, is directed to the photonic crystal fiber (PCF)(SCG-800, Newport Corp.) for the supercontinuum generation of the Stokes beam. A supercontinuum is formed when an intense laser pulse is focused into a nonlinear medium. The nonlinear processes act together to cause severe spectral broadening of the original pump beam.[37-38] The PCF used in this study is an index guiding PCF which consists of a high-index silica core and a micro-structured

cladding with a number of air-holes and arranged in a pattern that creates a hybrid air-silica material and with a refractive index lower than the solid core.[39-40] The Newport PCF is a polarization-maintaining PCF designed for zero-dispersion at 750 nm and with a core-diameter of 1.8 μm.

The beam splitter and a steering mirror are used to align and level the beam parallel to the axis of the PCF to achieve a high coupling efficiency. In addition to this, a high NA objective (M-40X, Newport Corp.) is used to focus the beam to the facet of the PCF. The half-wave plate and polarizer placed before the focusing objective for the PCF, serve to attenuate the input laser power to the fiber since at high laser power it can damage the fiber. The holder for the PCF is also an essential part of the set-up because it plays a critical role in the stability and reproducibility in the supercontinuum generation.[37] The PCF in this set-up is mounted on a XYZ stage (562-XYZ-M, Newport Corp.) and allows the beam to be aligned parallel to the axis of the PCF. A 20x objective (M-20X, Newport Corp.) is placed after the PCF to collimate the output beam. Section 3.3.2.1 details the alignment procedure for the supercontinuum generation.

A long pass filter (FSQ-RG780, Newport Corp.) placed after the collimated supercontinuum selects the wavelengths to form the Stokes beam. Figure 3.5 shows the transmission spectrum for the longpass filter. A steering mirror directs the beam toward the delay line for the Stokes beam and a routing mirror then directs the beam to pass through the 780 nm razor edge long pass filter and recombines with the pump beam. Figure 3.6 shows the transmission spectrum for the 780 razor edge longpass filter. After careful alignment, the two beams are both directed to the entrance port of the microscope

and then towards the microscope focusing objective similar to the one described above for the pump beam.

### *3.2.2. Microscope*

A pre-existing Nikon TE2000S inverted microscope equipped with an epi-fluorescence attachment (Figure 3.7) microscope is used for the CARS set-up. The epi-fluorescence attachment was previously modified by removing the fluorescent light source and the illumination lens to expose the back port of the microscope for laser delivery.[41] Irises were also mounted in the epi-port to aid in beam alignment. After the beam enters the epi-port of the microscope, it passes through the filter wheel that holds the short pass dichroic filter (785DRSP, Omega Optical) which reflects the pump and Stokes beam and passes through the anti-Stokes signal.

From the dichroic mirror, the beams are directed towards the objective and are focused towards the sample. There are currently two objective lenses in the microscope, a Nikon 10x 0.06 NA objective with a 10.55 mm working distance and a Nikon 100x 1.30 NA oil immersion objective with a 0.20 mm working distance. For the CARS set-up, the 100x objective is used as it gives better resolving power because of its high numerical aperture, as suggested from this simple resolution equation[24]:

$$R = \frac{\lambda}{2NA} \tag{3-1}$$

where R is the resolution, NA is the numerical aperture of the objective and λ is the wavelength of the light. The immersion oil used for focusing the excitation beams is a non-fluorescent type DF immersion oil. A cover slip which supports the sample must be

in contact with the immersion oil when focusing the sample image. The cover slips must be #1.5 type, with an average thickness of 0.15 and 0.19 mm, to match the working distance of the objective and the thickness of the cover slip. The cover slip with the sample is then placed in the slide holder mounted on a micrometer-controlled linearly encoded microscope stage (Nikon, model T-SR).[41] The travel distance for the microscope stage is 70 mm in the latitudinal direction (X) and 50 mm in the longitudinal direction (Y). A Boeckler Instruments Microcode II is connected to both the latitudinal and longitudinal encoders to show and record the position of the microscope stage through a digital readout.

The backscattered signal is collected by the same 100x objective lens which passes through the shortpass dichroic mirror and towards the side exit port of the microscope. The image is focused using white light from the lamp of the microscope. The image is viewed using the eyepiece or in the computer output using the Nikon camera (DS-Fi1, Nikon) mounted on the side-exit port of the microscope. Using the Basic Research software the dimensions of the sample image can be measured by using a micrometer slide to calibrate the Nikon camera.

### *3.2.3 Detection System*

The schematic for the signal collection set-up of the CARS microscope is shown in Figure 3.8. The backscattered light from the side exit port of the microscope passes through a BK7 biconvex focusing lens (LB1889, d = 50.8 mm, f = 250 mm, Thorlabs) to refocus the light. A periscope is then used to match the height of the exit port of the

microscope which is located at about 3.5 inches off the table, to the height of the entrance slit of the monochromator at about 4.8 inches off the table.[41] The periscope consists of two two-inch mirrors (BB2-E02, Thorlabs) on a kinematic mirror mount attached to the mounting post (P14, Thorlabs). The light passes through a short pass filter (SP01-785RU-25, Semrock) to block the exciting beams. The short pass filter is slightly tilted to shift the cut-off wavelength and effectively block the exciting beams. The transmission spectrum of the shortpass filter is shown in Figure 3.9. After the filter, the light is focused using a lens (LA1134, Thorlabs) to the entrance slit of the monochromator. Section 3.3.4 details the alignment procedure for the alignment of the signal collection set-up.

The detection system consists of an electron multiplying charged coupled device (EMCCD) attached to an Andor Shamrock monochromator SR-303i. The monochromator has a Czerny-Turner arrangement and is pre-aligned and pre-calibrated by Andor and equipped with interchangeable, computer controlled triple grating turret to optimize wavelength coverage and resolution.[42] The three gratings currently installed are 300, 600 and 1200 grooves/mm blazed at 500 nm. An Andor Newton EMCCD (DU971N-UVB, 1600 X 400 pixel array, 16 μm square pixels, back illuminated) then collects the CARS signal. The EMCCD can be thermoelectrically cooled to -80º C to minimize dark current.[41] The Andor Newton EMCCD detector has a 95% peak quantum efficiency as shown in Figure 3.10 and is optimized for ultra-low light level spectroscopy applications. EMCCD's are appropriate for applications that generates low signal and when shorter exposure times and faster spectral rates are desired. The CARS spectra is

acquired using Andor Technology's Andor Solis control and analysis software with a dashboard that controls the functionality of the monochromator, such as the entrance slit width, grating and wavelength selection and calibration. The entrance slit width is varied depending on the intensity of the CARS signal. To achieve a better resolution, the 1200 grooves/mm grating is used for most of the acquisitions and the CCD chip is set to full vertical binning mode (FVB) to improve signal to noise ratio and faster readout speeds.

### *3.3 Laser and Instrument Alignment*

The alignment of the entire CARS set-up is critical in optimizing the laser power at the microscope, the generation of the supercontinuum for the Stokes beam and to a strong CARS signal. There are three areas where alignment of the beams is important: the supercontinuum generation, the area where the pump and Stokes beam overlap towards the entrance port of the microscope, and the signal detection area. The remainder of this section will discuss the alignment and calibration of the set-up, especially with the supercontinuum generation, and other individual components.

#### *3.3.1 Overlap of Pump and Stokes Beam*

As shown in Figure 3.1, the pump beam recombines with the Stokes beam after reflection from the 780 nm RELP long pass filter. At this point, it is important that the beams overlap. A strong CARS signal is generated when the two beams overlap in space and time. Using two mirrors and two irises, a straight laser line beaming into the microscope epi-port and overlapping beams are assured. To align the pump beam, the

first iris is placed just after the RELP filter, the routing mirror just before the RELP filter is adjusted to center the beam at the iris. The second iris is placed a few inches away from the RELP filter and is adjusted to center the beam at the second iris. For the Stokes beam, using the same irises, the routing mirror is adjusted after the collimating objective of the PCF for the first iris, and the routing mirror before the RELP filter for the second iris. This then assures spatial overlap, as both the beams passes through the center of the iris.

A periscope is placed before the entrance port of the microscope to match the height of the incoming beams to the height of the entrance port. To ascertain the overlapping of two beams at the objective's entrance aperture, the objective revolving nosepiece is rotated to an empty spot that does not have an objective lens. A white sheet of paper is replaced and marked on the center of the objective mounting hole. The iris built for the epi-fluorescence attachment is closed until the opening is slightly larger than the beam diameter. The bottom mirror of the periscope is adjusted until the beam is at the center of the opening of the iris. The iris is opened and the top mirror of the periscope is adjusted until the beams are hitting the central mark of the white sheet of paper. The process is repeated until the two beams hit the center of the iris and the mark. At this point, if the beams are properly aligned, they should overlap. If the beams are slightly shifted, then the RELP filter is slightly adjusted for the pump beam and the routing mirror just before the RELP filter for the Stokes beam.

### *3.3.2 Supercontinuum Generation*

The broad Stokes beam needed for this multiplex CARS set-up is based on the generation of supercontinuum from a photonic crystal fiber (PCF). Supercontinuum generation is the formation of broad continuous spectra by focusing high power pulses through a nonlinear material.[43] Coupling an ultrafast laser pulse directly into a PCF produces bright light with broad spectral coverage which made PCF technology find its application in other nonlinear spectroscopy techniques. Unlike standard optical fibers which guide light by total internal reflection between a core with high refractive index and a cladding with low refractive index, the index differences in PCF's are obtained by a forming a hybrid material with high and low refractive index and constructed in a structure similar to that found in certain crystals, hence the name photonic crystal fiber.[43] The PCF used in this application is an index guiding PCF wherein the core is a solid glass with a high index and embedded in an air-filled cladding structure. Standard PCF's have cores with 1-2 μm in diameter and because they have the ability to confine light into this hollow core, the pulse interactions with the fiber is highly nonlinear and result to several higher order nonlinear processes that contributes in the supercontinuum generation.[43]

#### *3.3.2.1 Supercontinuum Generation Set-up Alignment*

Using the beamsplitter and the steering mirror, the beam is aligned by following the hole pattern at the optical table where the translation stage is installed. The height of the beam is adjusted to match the height of the XYZ translation stage and the optical axis of the fiber. The half-waveplate and the Glan laser polarizer are installed and the laser

power set to 50 mW by rotating the half-waveplate and placing a power meter after the polarizer. It is very important not to exceed 50 mW laser power when optimizing or aligning to avoid damaging the fiber. The stage (561D-YZ, Newport Corp.) is installed for the focusing objective assembly and the objective lens is removed. A white paper is placed about 5 inches away and the beam position is marked. The focusing objective is then replaced and the XZ stage of the focusing objective is adjusted to center the beam to the target. On the other hand, the XYZ stage for the fiber is installed and the line marking the polarization direction is aligned parallel to the polarization of the beam. The XYZ stage is adjusted to bring the tip of the focusing objective lens closer and centered at the input facet of the fiber. For 20x and 40x focusing objective, the distance between the tip of the objective and the input facet of the fiber should be approximately 5 mm and 0.5 mm respectively. A white paper is placed about 5 inches away from the fiber and the beam is aligned to pass through the fiber and the transmitted beam is observed using an IR viewer on the white paper. The vertical and horizontal axes of the stage are alternately fine tuned until the central spot is minimized and completely diminished and an evenly diffused light is observed. The X axis of the stage along the optical axis of the fiber is adjusted to focus the beam into the fiber core and improve the throughput. Generally, at 50 mW input and 25 % coupling efficiency, a visible red light is observed. The steering mirrors can also be fine adjusted to improve the throughput. Once an even supercontinuum is generated, the input power can be increased and fine tuning the XYZ alignment, the output beam is optimized which causes the color of the beam to change. The collimating objective assembly (462-XY, Newport Corp.) is installed using a 20x

objective lens. The collimating objective stage is adjusted to collimate and adjust the size of the output beam.

Based on Newport's application note for the SCG-800 fiber, the properties of the generated supercontinuum are strictly defined by the amount of the coupled power rather than the coupling efficiency.[37] Coupled power is the measured power after the collimating objective and coupling efficiency, on the other hand, is the ratio of the power measured after the collimating objective and the power before the focusing objective. For a 40x focusing objective lens, 48% efficiency was observed at 200 mW input power and 97 mW of coupled power. Figure 3.11 shows the appearance of the beam at 48 mW and 200 mW input power at about 48% efficiency and Figure 3.12A and 3.12B show the supercontinuum spectra obtained at 50 mW and 200 mW input power, respectively. At higher input power the supercontinuum spectrum broadens and can extend at longer wavelengths compared to the spectrum obtained using lower input power.

### *3.3.3 Calibration of Detector and Microscope*

Calibration of the detector is an important first step before acquiring spectrum from a sample since it ensures accurate location of peaks in a spectrum. Calibration of the instrument can be done using a fluorescent light. An optical fiber (AFS1051254, Thorlabs) is used to collect the light from the fluorescent lamp to the monochromator by mounting the collimating end of the fiber to the monochromator entrance slit and the other end of the fiber pointed under the fluorescent lamp. In the Andor dashboard, the entrance slit is set to 10μm and acquisition time to 0.5 seconds. The 300 grooves/mm

grating is selected and the center wavelength is set to zero in the wavelength drive control to allow all the light that enters the monochromator directed towards the CCD camera. When the center wavelength is set to zero, the unit for the x-axis is changed to pixels. The ***Display*** button is selected from the offset adjustment control toolbar. At the ***grating*** offset tab located at the offset adjustment toolbar, the centre line button is selected and a red line appears at 800 pixels. Signal is acquired and a sharp peak should ideally appear close to the red line. If the peak is not centered at 800 pixels, the offset value is adjusted by pressing the appropriate + or – offset adjustment buttons to bring the center of the peak onto the red line.[44] The adjustment step size may be changed from a drop down list. Figure 3.13 shows the spectra before and after grating offset adjustment. The grating angle is set so that the detected region includes the 404.9 nm, 435.8 nm and 546.0 nm peaks from fluorescent light. With the other end of the fiber pointed at the fluorescent light, signal is acquired and the three peaks mentioned are located. The wavelength of the peaks should be as close as possible to the reference value. If the peaks are significantly shifted, the offset adjustment value is changed until the peaks shifts to their correct value. The calibration procedure is repeated for the 600 grooves/mm and 1200 grooves/mm grating.

### *3.3.4 Signal Collection Alignment*

After calibrating the detector, the signal beam is sent to the detector by directing and properly aligning the signal beam from the microscope side exit port to the entrance slit of the monochromator. The backscattered epi-CARS signal exits the side-port of the

inverted microscope and must be properly aligned into monochromator to prevent losing signal from clipping into optics. The collected white light from the condenser can be used first in aligning the signal beam. First, the condenser is turned on and the light is collected using the 100x objective lens. The collected white light then exits the side port of the microscope and is diverging. A biconvex lens is placed at the side exit port and centered about the exiting signal beam. Two irises along the path of the signal beams are placed and the height adjusted such that they match the height of the exit port of the microscope from the optical table. The tilt and position of the lens are adjusted to ensure the signal beam is passing through the center of both irises. The periscope is placed, which consists of two two-inch mirrors, to bring the beam up and match the height of the entrance slit of the monochromator. Two irises are placed along the intended path of the signal beam and the alignment of the beam is ensured by adjusting the bottom mirror of the periscope to center it the hole of the first iris and adjusting the top mirror of the periscope to center it the hole of the second iris. The process is repeated until the signal beam passes through the center of both irises. A shortpass filter and focusing lens are placed before the monochromator, making sure that the focal point of the lens is at the entrance slit of the monochromator. After aligning the signal collection optics with white light and making sure the signal beam enters the monochromator, the objective is focused on an empty cover slip. The white light source is turned off and the pump and Stokes beam are allowed to pass through the objective. Using an IR viewer, the signal beam that exits the side port of the microscope is observed and the alignment of the beam is ensured and doesn't clip on any optic. The Andor software is opened and the CCD camera

temperature set to -80° C to minimize thermal noise and the center wavelength set to 780 nm at the wavelength drive control. The acquisition time is set to 0.02 seconds and slit width to 10μm to avoid saturating the CCD camera and the spectrum. To efficiently block the pump and Stokes beam using the 785 nm shortpass filter, the filter is slightly tilted. Tilting the filter increases the angle of incidence from normal and the features of the spectrum shifts to shorter wavelengths.[45] The real time acquire signal button is selected and while observing the spectrum, the 785 nm shortpass filter is slowly tilted until the peak for the pump beam disappears. The slit width is changed to 50μm and the acquisition time to 5 seconds and a signal is acquired. A peak at 780 nm should be observed for the pump beam. The shortpass filter is slowly tilted and a signal is continuously acquired until the peak for the pump beam is attenuated. The black box is placed to cover the signal collection part of the set-up to minimize stray light photons in entering the CCD camera.

#### 3.3.4.1 Testing Signal Collection Alignment

To test whether the signal collection optics and detection system are set-up correctly and able to detect a signal from the sample, the microscope is converted to a spontaneous Raman microscope as shown in Figure 3.14. This is done by using a 785 nm diode laser (PI-ECL-785-300-SH, Process Instrument), a dichroic longpass filter (820DRLP, Omega Optical) inside the microscope filter wheel to reflect the exciting beam and transmit the signal, and a Razor Edge longpass filter (XR3004793 ALP, Omega Optical) to block the exciting beam before the detector. A naphthalene sample is

used to test the set-up and obtain a Raman signal detected by the CCD detector. Figure 3.15A shows the spectrum of naphthalene from literature and Figure 3.15B shows the obtained naphthalene spectrum using this set-up with 10 seconds acquisition time, 300 groove/mm grating and ~ 300 mw of laser power. The location of the peaks observed in the naphthalene spectrum agrees well with the reference spectrum. By successfully generating a Raman spectrum of naphthalene, this ensures proper alignment of signal collection set-up for efficient epi-detection of signal from the microscope stage.

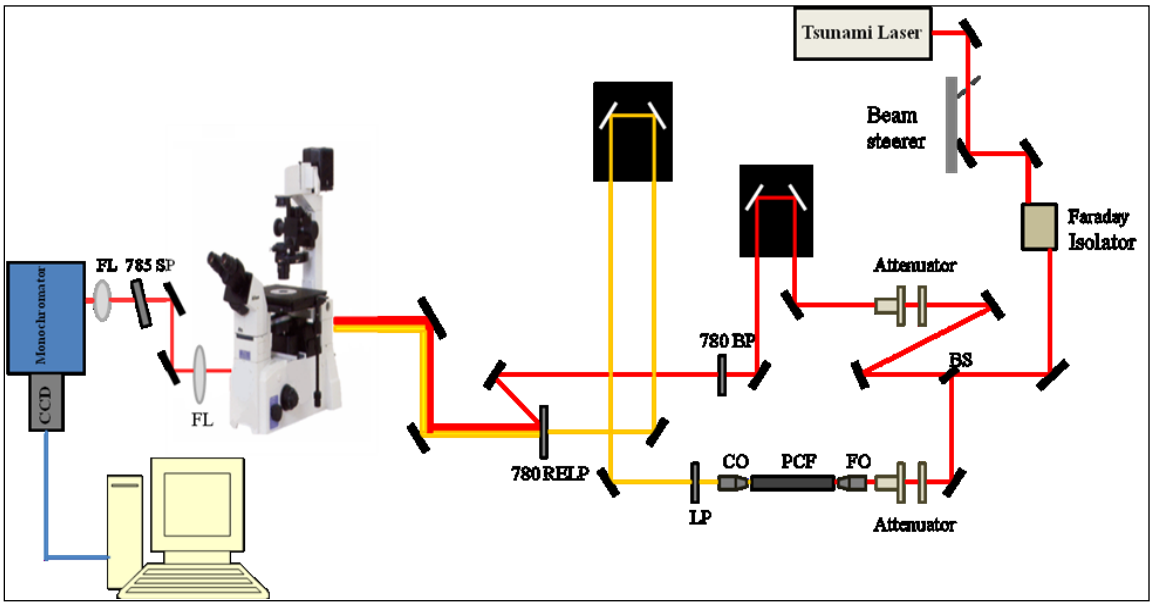


**Figure 3.1:** Schematic diagram of the CARS microscope set-up. BS – beamsplitter, FO – focusing objective, PCF – photonic crystal fiber, CO – collimating objective, LP – longpass filter, 780 BP – 780 nm bandpass filter, 780 RELP – 780 nm razor edge filter, FL – focusing lens, 785 SP – 785 nm shortpass filter.

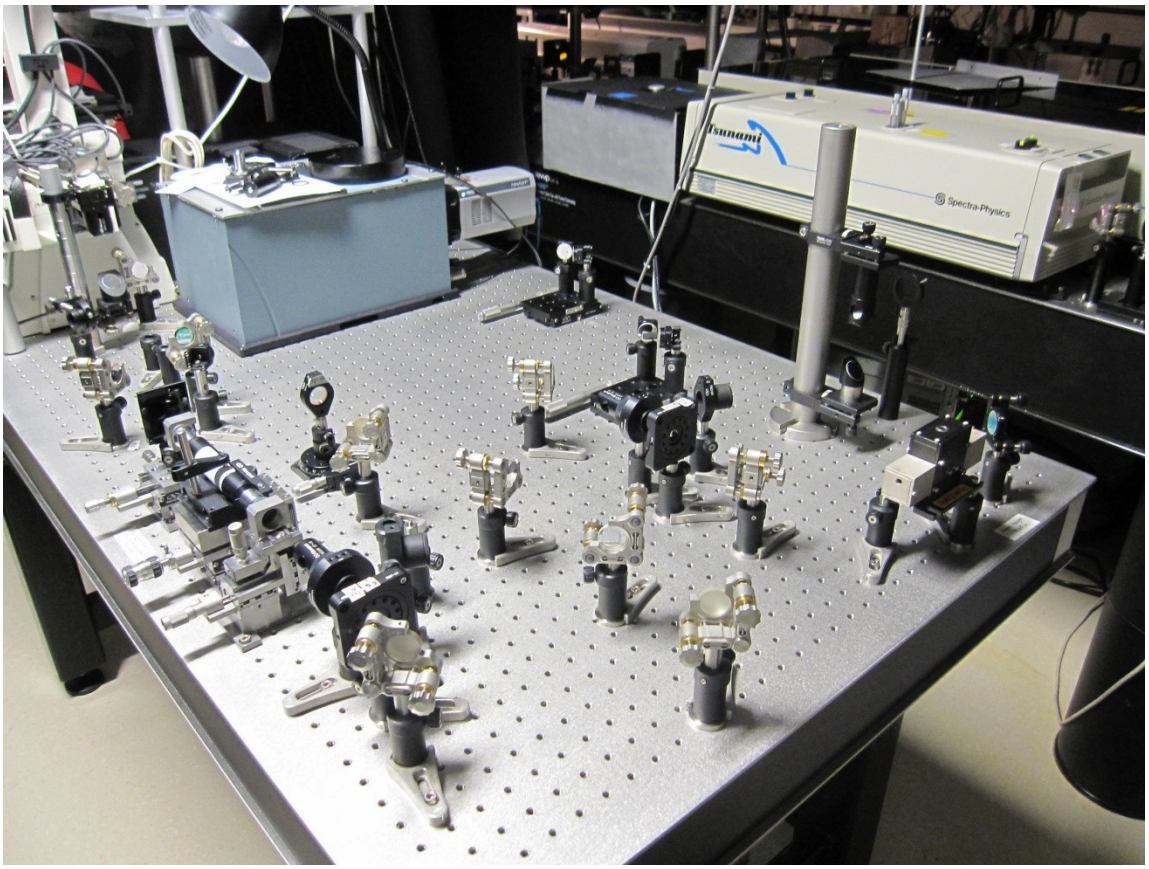


**Figure 3.2:** Actual CARS microscope set-up.

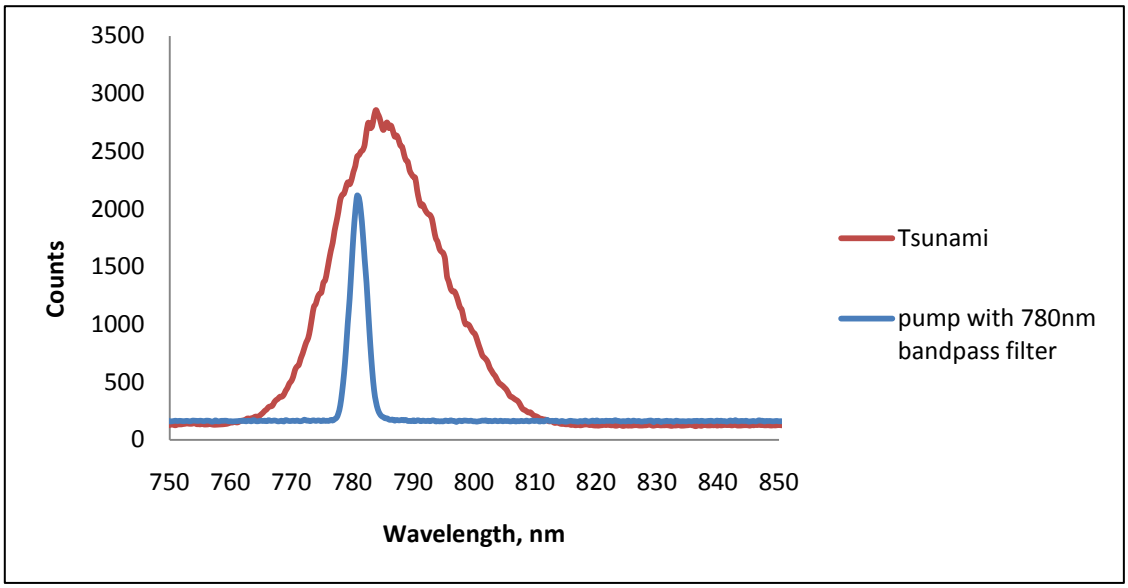


**Figure 3.3:** Spectrum of the beam directly from the Ti:Sapphire laser and the narrow bandwidth pump beam.

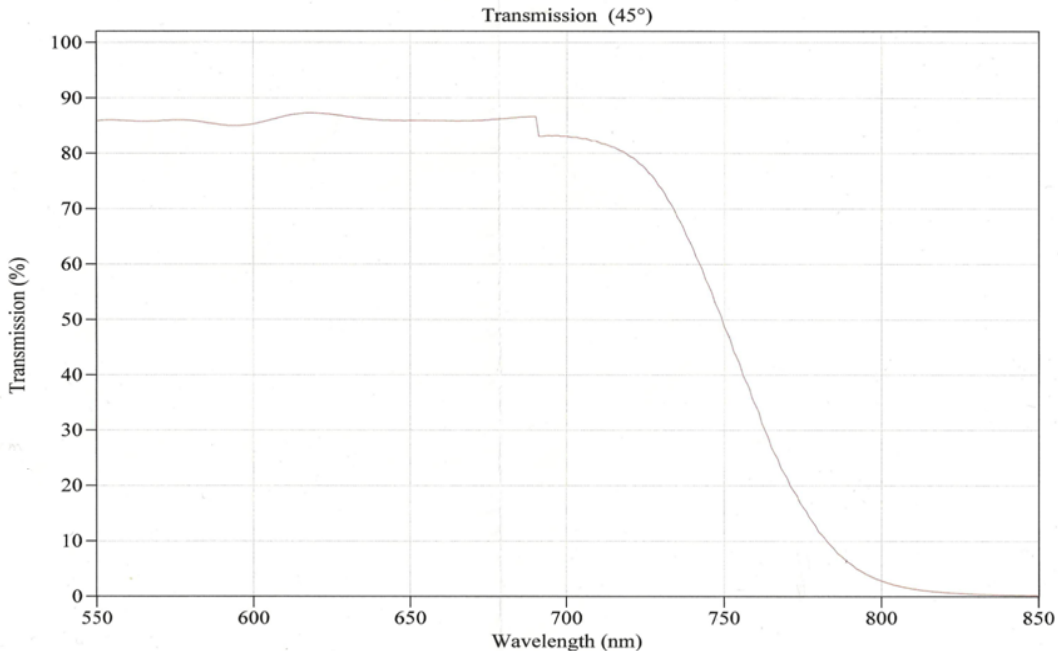


**Figure 3.4:** Transmission spectrum for the 785 nm dichroic shortpass filter. Spectrum obtained from Omega Optical.

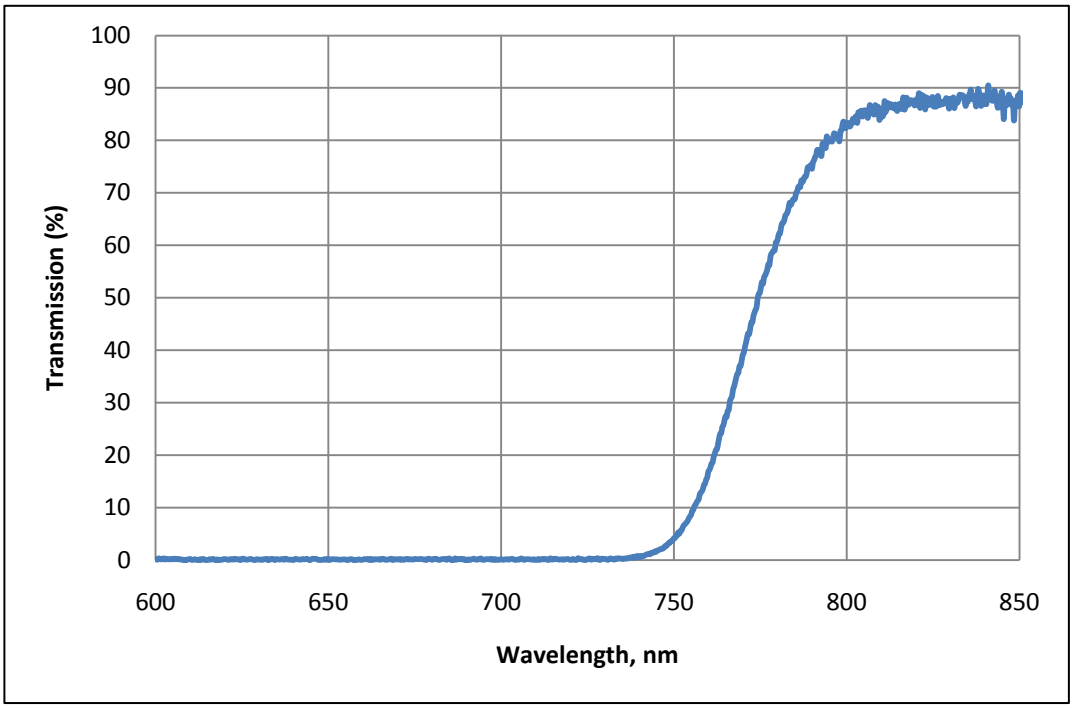


**Figure 3.5**: Transmission spectrum for the RG780 longpass filter.

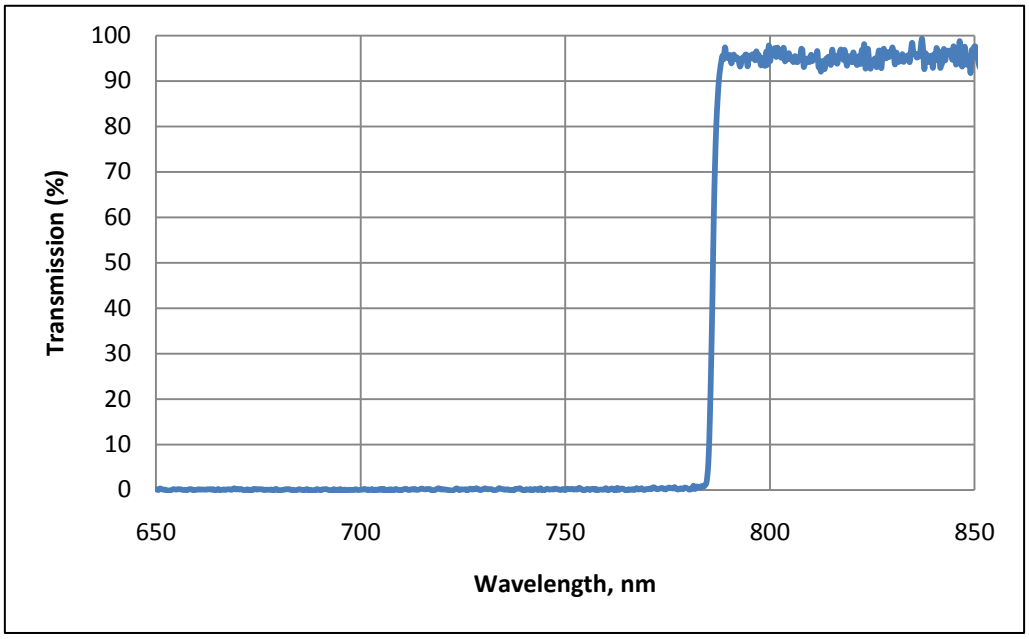


**Figure 3.6:** Transmission spectrum for the 780 nm Razor Edge longpass filter.

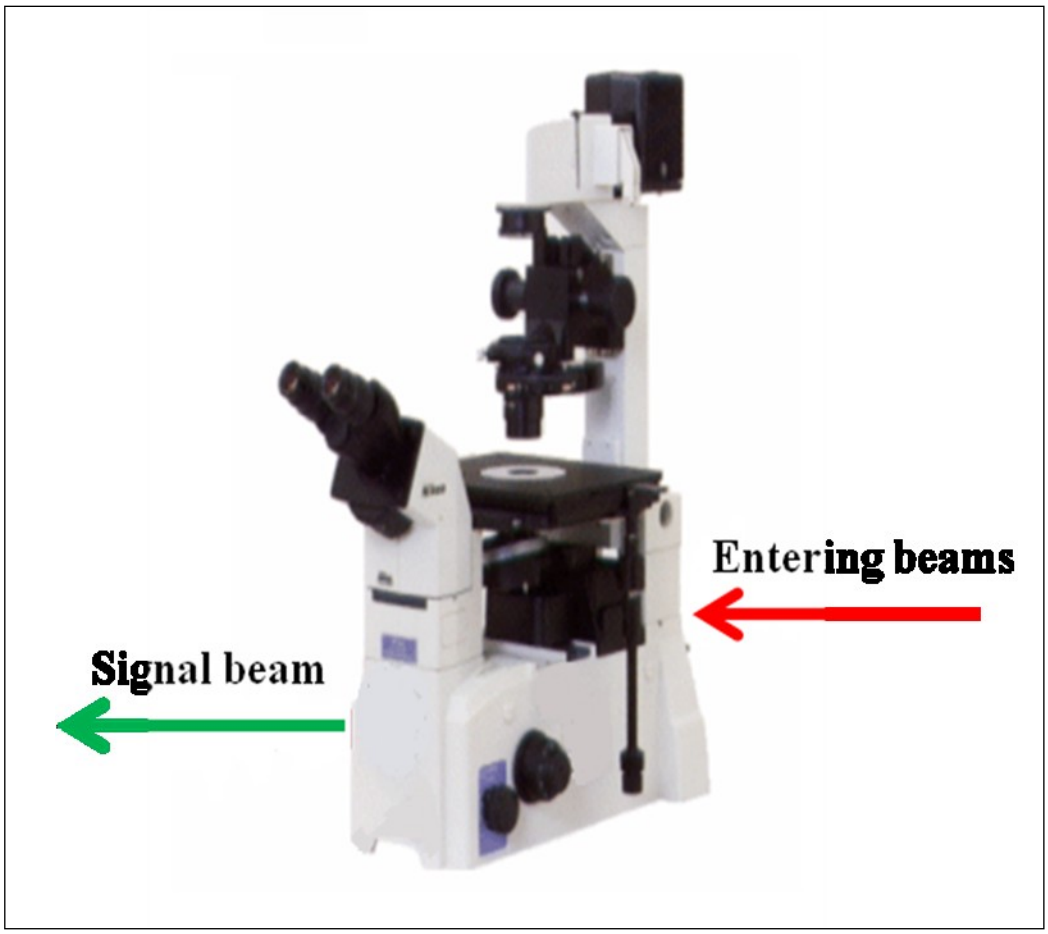


**Figure 3.7:** Nikon Eclipse TE2000S microscope. (Photo courtesy of Nikon.com)

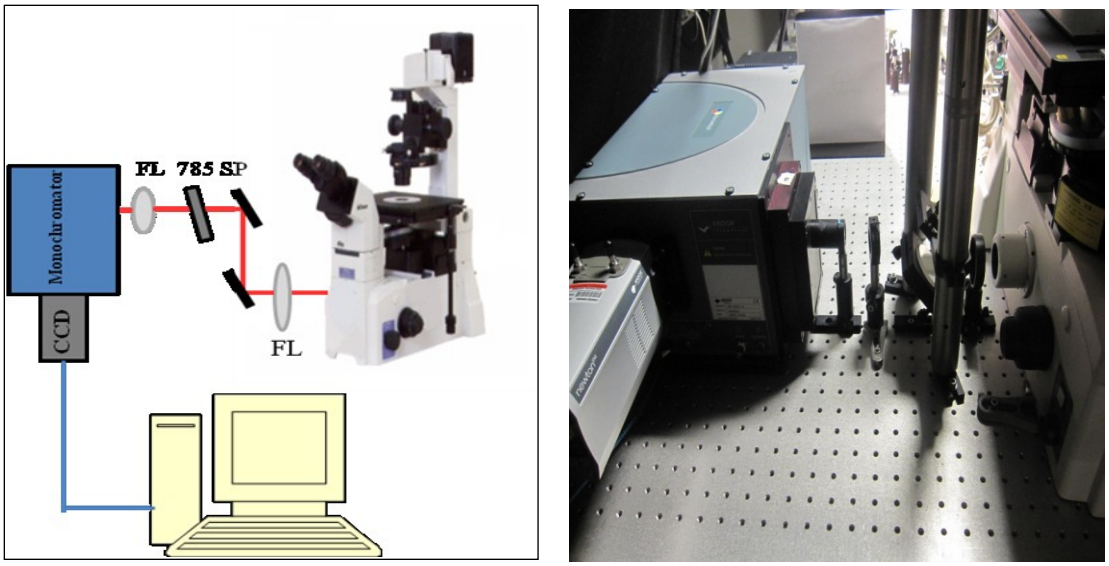


(A) (B)

**Figure 3.8:** Signal Collection Set-up. (A) Schematic of the signal collection part of the CARS set-up (B) Actual signal collection set-up.

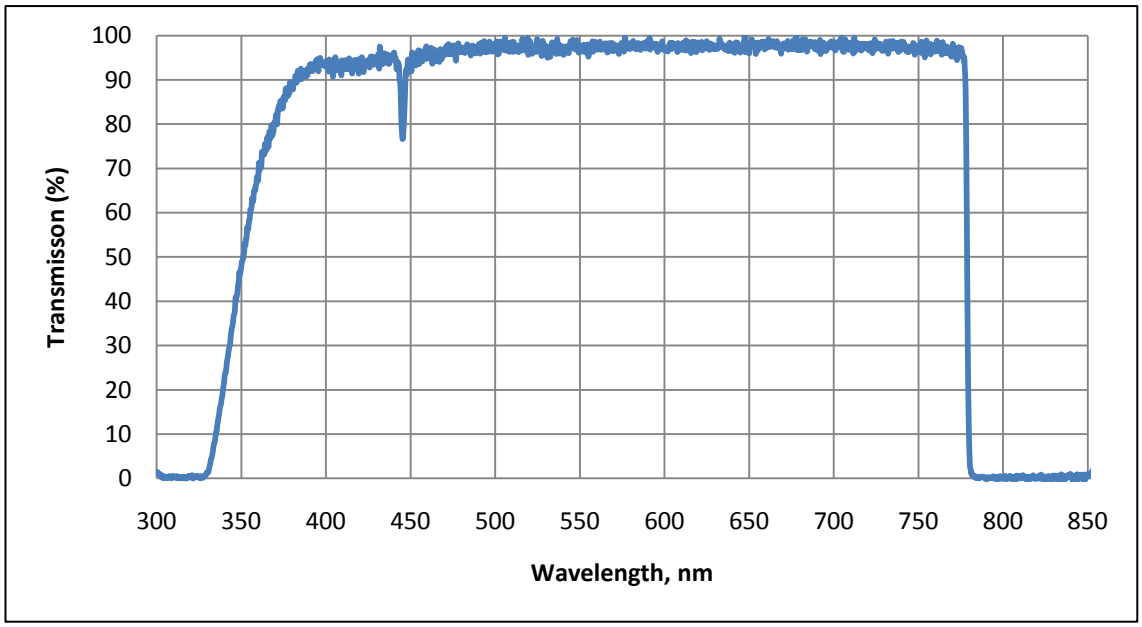


**Figure 3.9:** Transmission spectrum for the 785 nm shortpass filter.

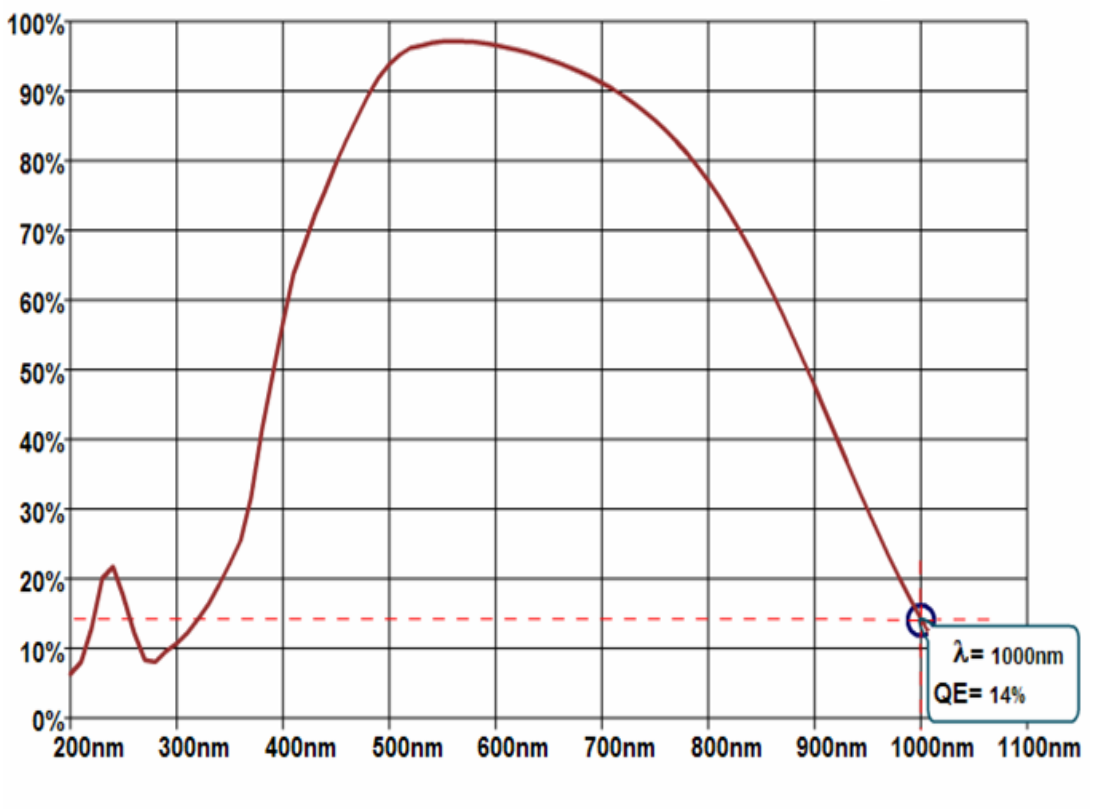


**Figure 3.10:** The EMCCD quantum efficiency curve. The efficiency curve is obtained from *www.andor.com*

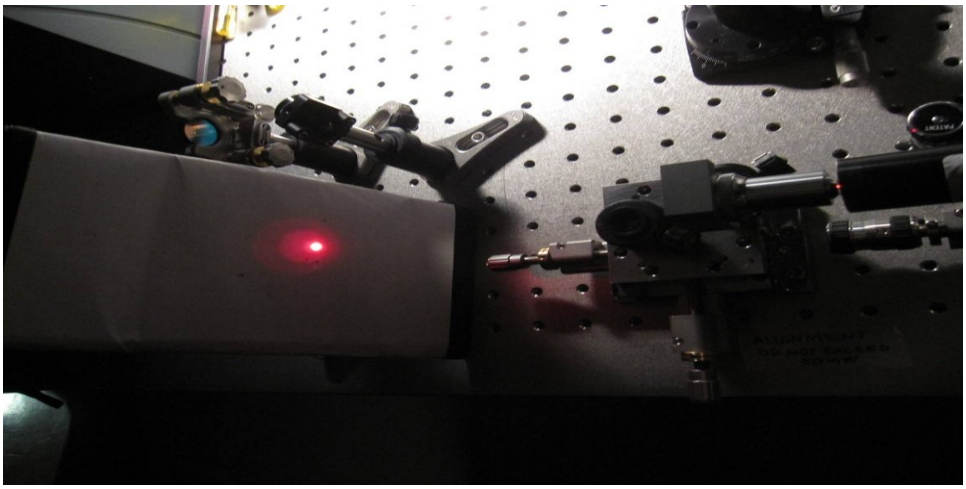

(A)

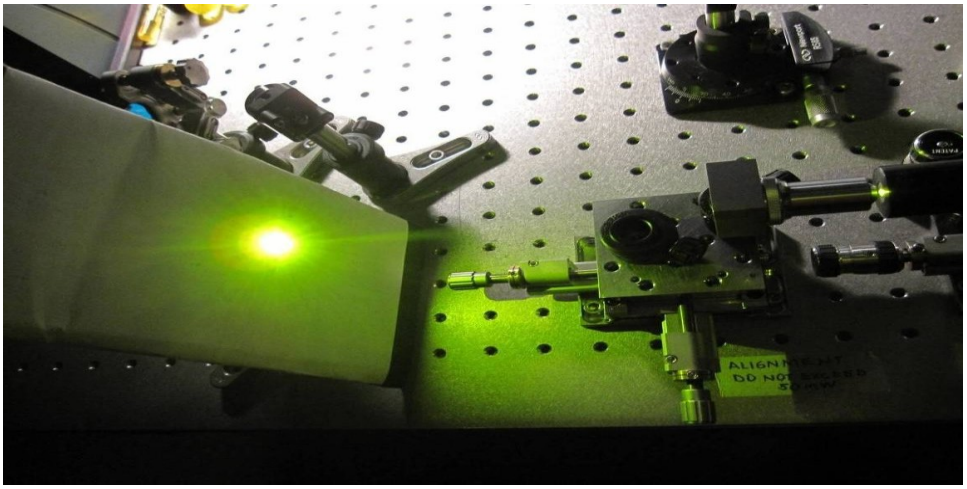

(B)

**Figure 3.11:** Supercontinuum Beams. (A) Supercontinuum beam at 48 mW input and 48% coupling efficiency. (B) Supercontinuum beam at 200 mW and 48% coupling efficiency.

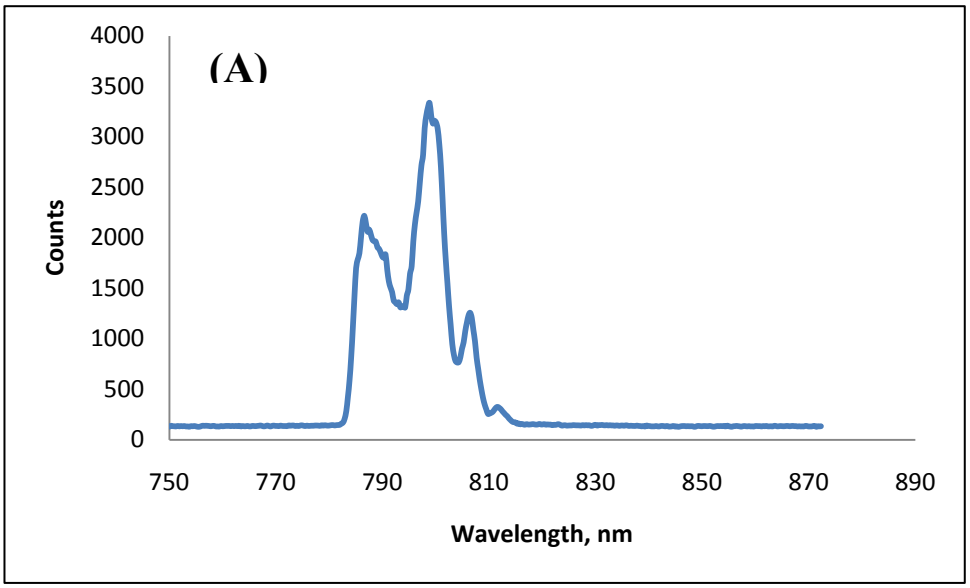


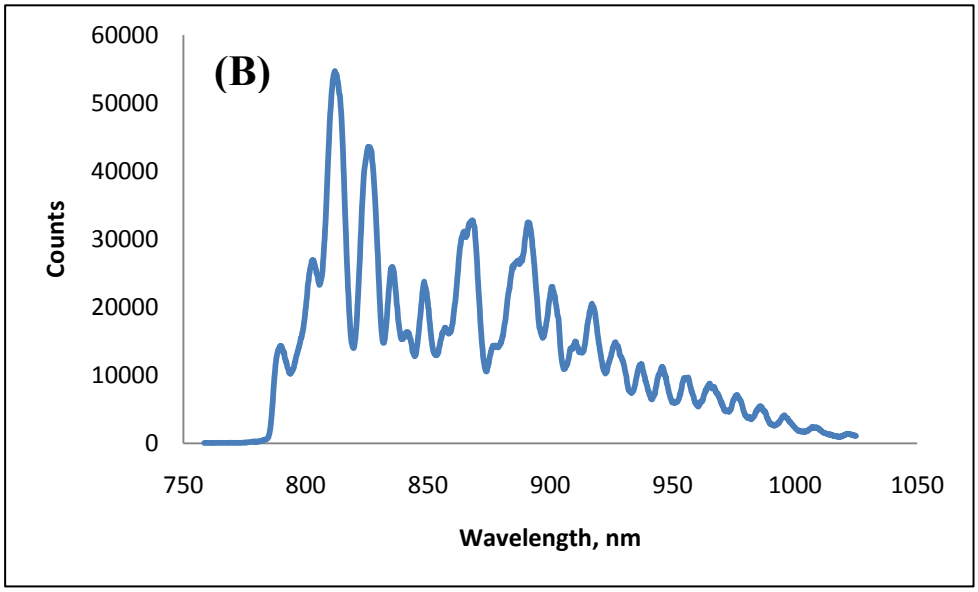


**Figure 3.12:** Supercontinuum spectra. **(A)** Supercontinuum spectrum generated with 50 mW input power and ~48% coupling efficiency. **(B)** Supercontinuum spectrum generated with 200 mW input power and ~48% coupling efficiency.

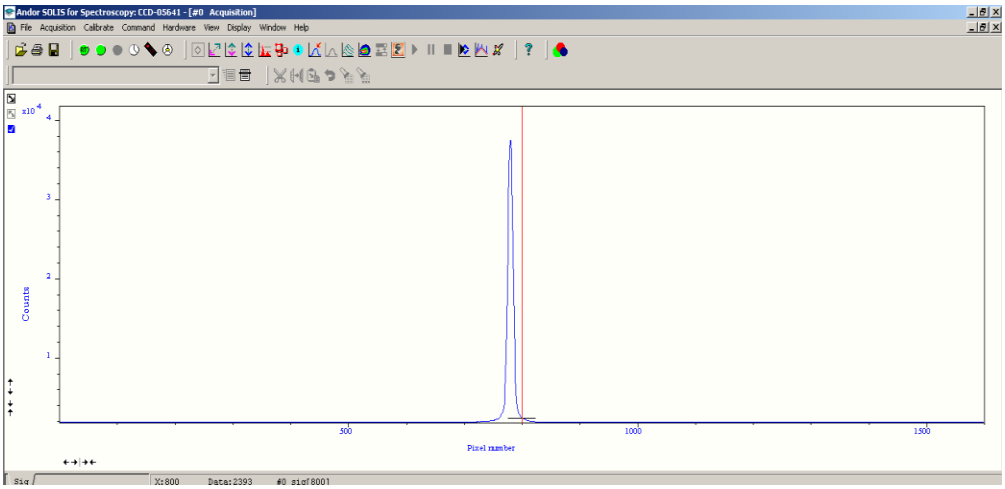


(A)

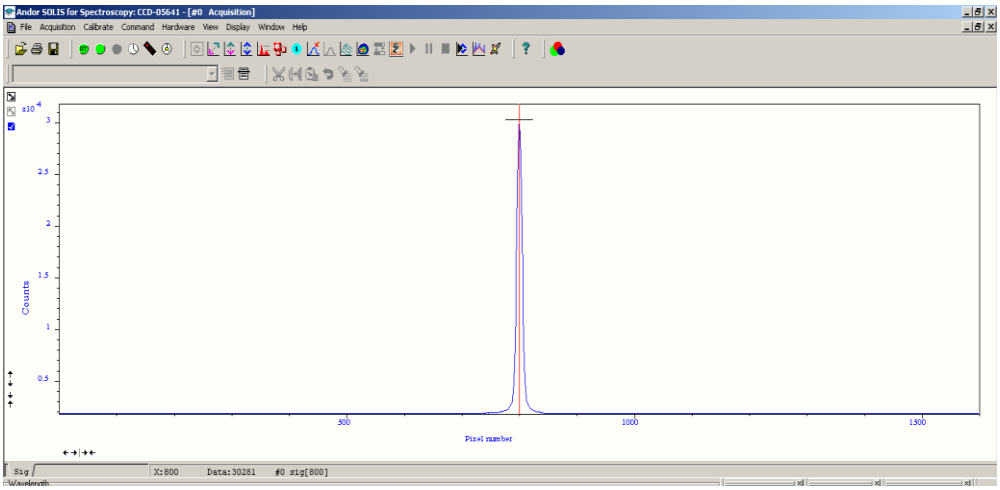


(B)

**Figure 3.13:** (A) Spectra before grating offset adjustment. (B)Spectra afer grating offset adjustment.

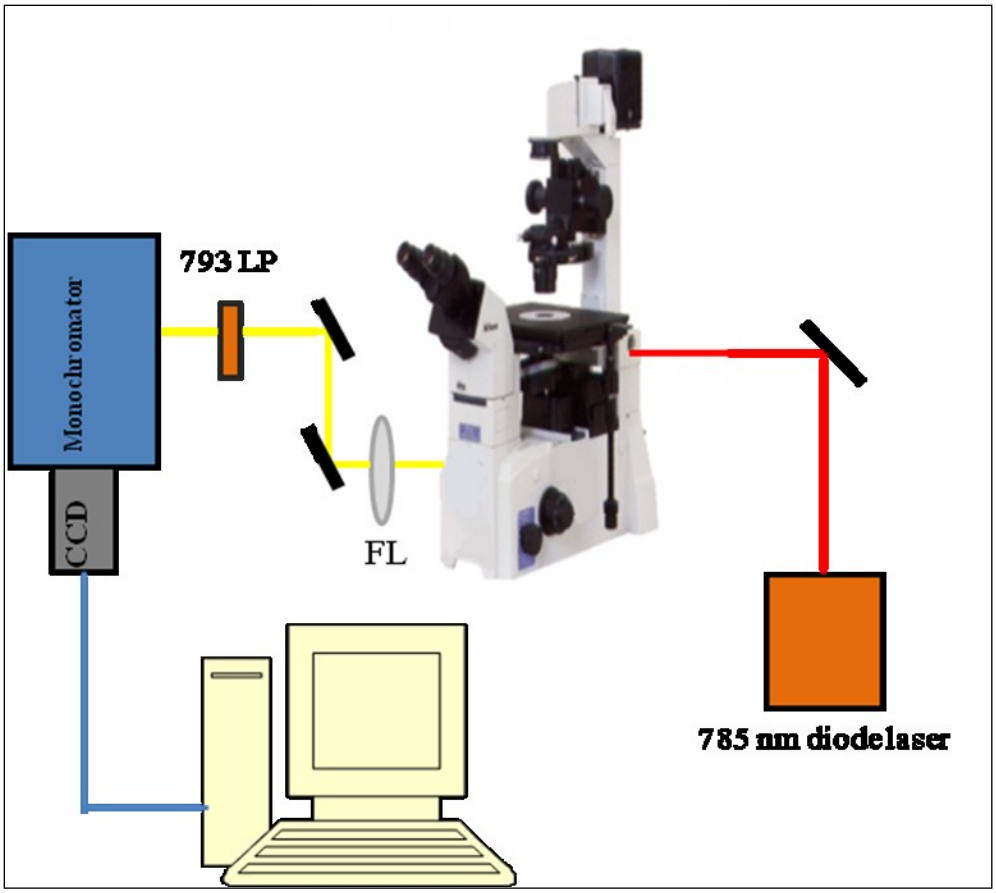


**Figure 3.14:** Raman Microscope Schematic Diagram.

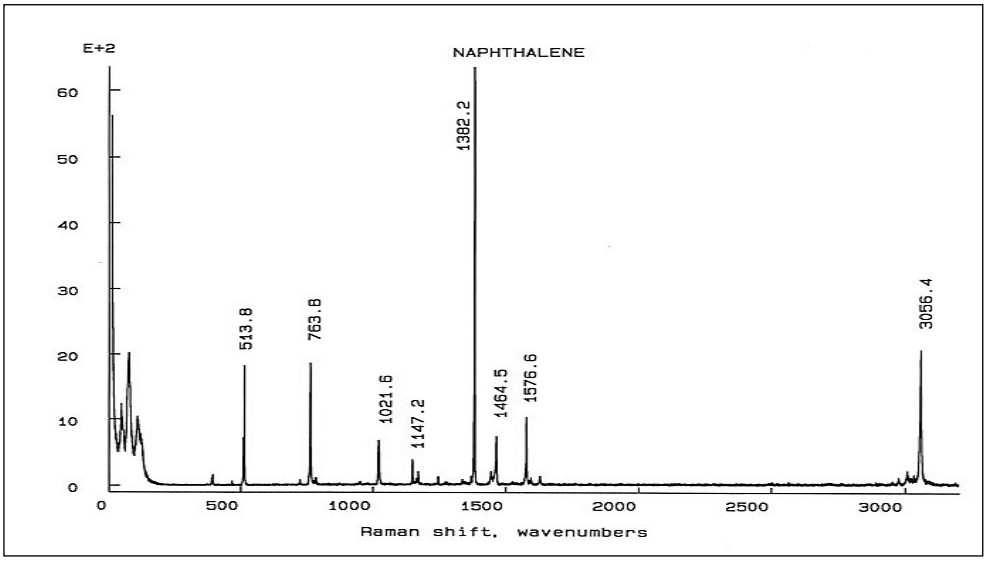


**(A)**

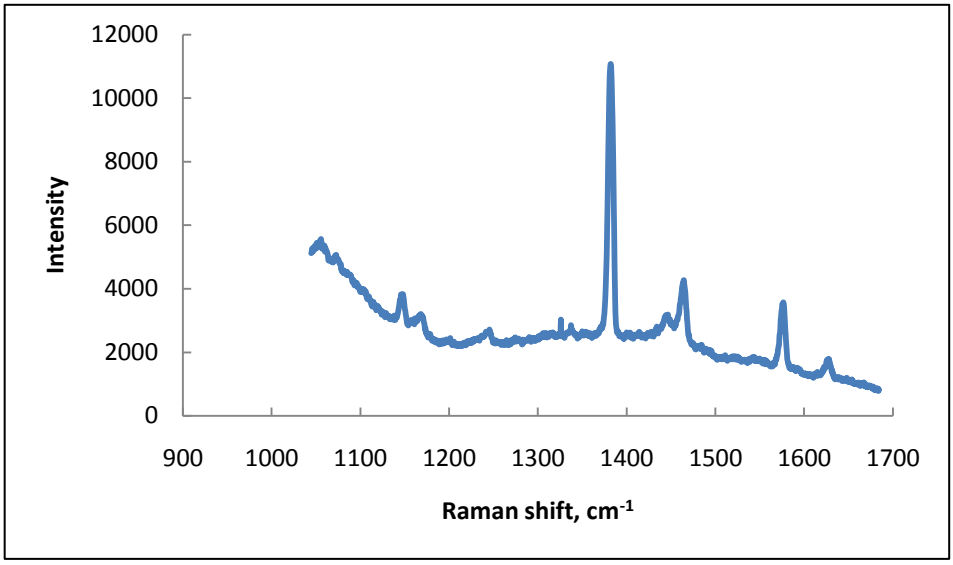


**(B)**

**Figure 3.15: (A)** Reference Spectrum of Naphthalene[46] **(B)** Background-corrected Raman spectrum of naphthalene.

# CHAPTER 4

# RESULTS AND DATA

## 4.1. Finding the Zero-Delay Point

One condition for generation of a CARS signal is the spatial and temporal overlap of the two exciting beams. To ensure spatial overlap, two irises were placed after the RELP filter, and the beams were aligned such that both beams pass through the center of the iris. To set-up the correct timing between the pump and the Stokes beam, the optical path lengths of either beams were measured first using a measuring tape. Additional lengths equivalent to about half the length or thickness of any optic along each beam path were added to that particular path length because beams experience retardation as they pass through any optic. After measuring the optical path lengths, translation stages for the delay lines were adjusted to make the two path lengths equal.

To find the zero-delay point, a nonlinear optical crystal, Beta-Barium Borate (BBO), was used to observe the sum frequency signal generated when the two beams are focused at the crystal that are spatially and temporally overlapped. The BBO crystal used is a Type 1 BBO that is cut for 800 nm (Eksma Optics). Both the beams are set to vertical polarization and a 20x objective lens (M-20x, Newport Corporation) was used to focus

the beams to the crystal. A white card was placed about 5 inches away from the BBO crystal to observe the Second Harmonic (SH) and Sum Frequency (SF) signal that will be generated. Figure 4.1 shows the set-up for finding zero-delay point. The crystal is rotated to see the blue-colored SH of the pump beam and the broad green-colored SH of the Stokes beam. The crystal was set to an angle to equalize the intensity of the two SH spots. The delay lines are adjusted until the SF light is observed which is a flash of purple and blue color in between the two SH spots. The SF signal is optimized by adjusting the spatial overlap or the collimation of the Stokes beam.

### 4.2. Generation of Forward-CARS signal

For the initial generation of CARS signal, the generation of forward CARS signal using hexadecane was explored. Figure 4.2 shows the forward CARS detection set-up. A forward CARS signal from a bulk sample is stronger than an epi-CARS signal and is highly directional. This detection scheme will be able to generate a stronger CARS signal and can easily be detected. Hexadecane is used as the sample because of the strong signal generated at 2840 $cm^{-1}$ for the $CH_2$ symmetric stretch. For the forward CARS set-up, a 20x objective lens (M-20x, Newport Corporation) is used to focus the beams to the sample and a 10x objective lens (M-10x, Newport Corporation) to collect and collimate the signal beam. The signal is detected using either Ocean Optics spectrometer or directed towards the Andor spectrometer with CCD as the detector. To increase the power for the pump beam, the 780 nm bandpass filter was removed and a pump power of ~118mw was measured. By removing the bandpass filter, the power for

the pump beam is increased but a broad CARS signal peak is generated since the spectral resolution of the peak depends on the spectral bandwidth of the pump beam.

With the forward CARS detection set-up and hexadecane as sample, the $CH_2$ symmetric stretch is expected to peak at ~2840 $cm^{-1}$ (~639.6 nm) where the pump and the Stokes beam are set at 782 nm and 1002.5 nm, respectively. Figure 4.3A shows the CARS signal generated for the $CH_2$ symmetric stretch at 10 seconds acquisition time, 118 mw pump power and 38 mW Stokes beam power. Because the bandpass filter for the pump beam was removed, a broad CARS signal for the $CH_2$ symmetric stretch was observed. To ensure that the peak observed is a CARS signal, the signal peak disappeared completely when either the pump or the Stokes beam is blocked and also when the time delay stage is adjusted. This technique confirms that the peak signal observed is a real signal. Figure 4.3B and 4.3C shows the spectrum obtained when the Stokes and pump beam are blocked respectively. These spectra also show the contribution of a large background both from the pump and Stokes beam at the $CH_2$ signal region. To improve the background and lower the baseline, a second shortpass filter was added before the monochromator and the spatial and temporal overlap was optimized. This resulted to a spectrum with good signal to noise ratio even at 1 second acquisition time (Figure 4.4A). The pump and Stokes beam were then blocked alternately and time delay stage was adjusted to confirm the peak observed is a CARS signal. Figure 4.4B and Figure 4.4C respectively shows the spectrum obtained when the Stokes and pump beam are blocked which confirms the CARS signal. A spontaneous Raman spectrum was also obtained (inset of Figure 4.4A) for the hexadecane sample and

the spectral profile is similar to the CARS spectral profile which confirms that the CARS signal obtained is from the $CH_2$ symmetric stretch. Further optimization of the set-up and improve filtering of the exciting beams can still lower the baseline and lessen the background at the signal detection region.

After the generation of the forward CARS signal, the next step is to send the two beams into the microscope and generate an epi-CARS signal. At present, the system is being optimized for epi-detection to generate a strong CARS signal with better spectral resolution and good signal to noise ratio.

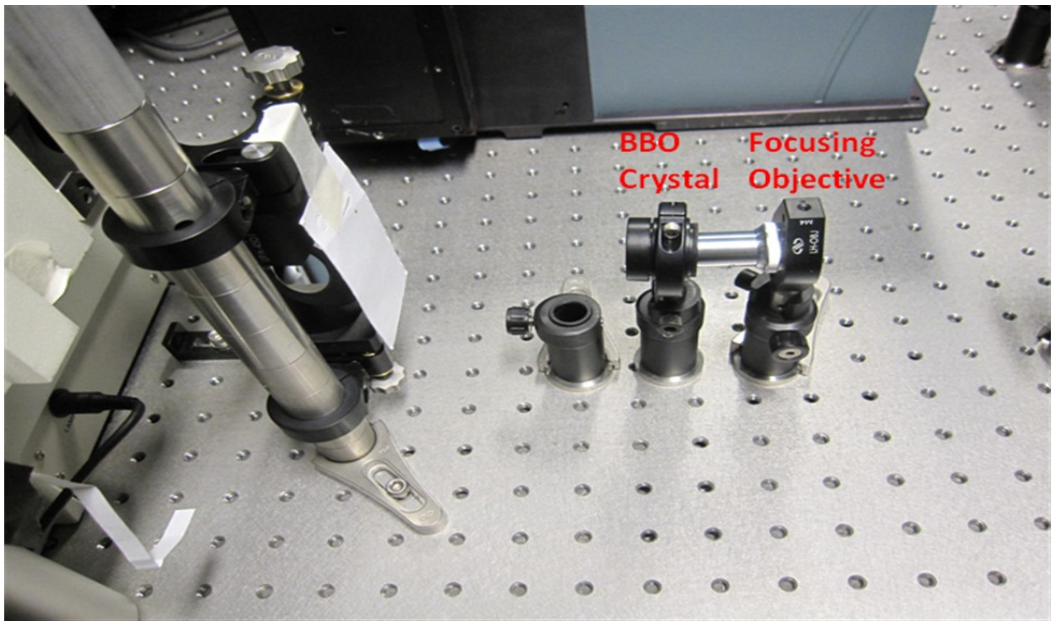


**Figure 4.1**: Set-up for finding the zero-delay point.

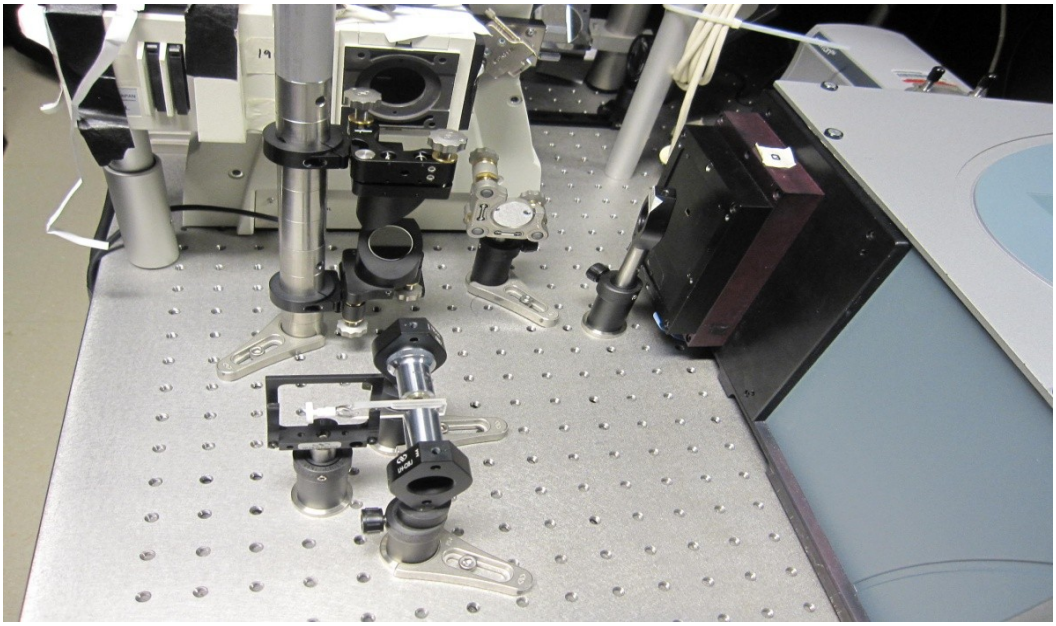

**Figure 4.2:** Forward CARS signal detection set-up. The collimated beam is sent straight to the Andor Spectrometer for detection. A beam steerer is used to bring the beam towards the entrance slit of the Andor spectrometer.

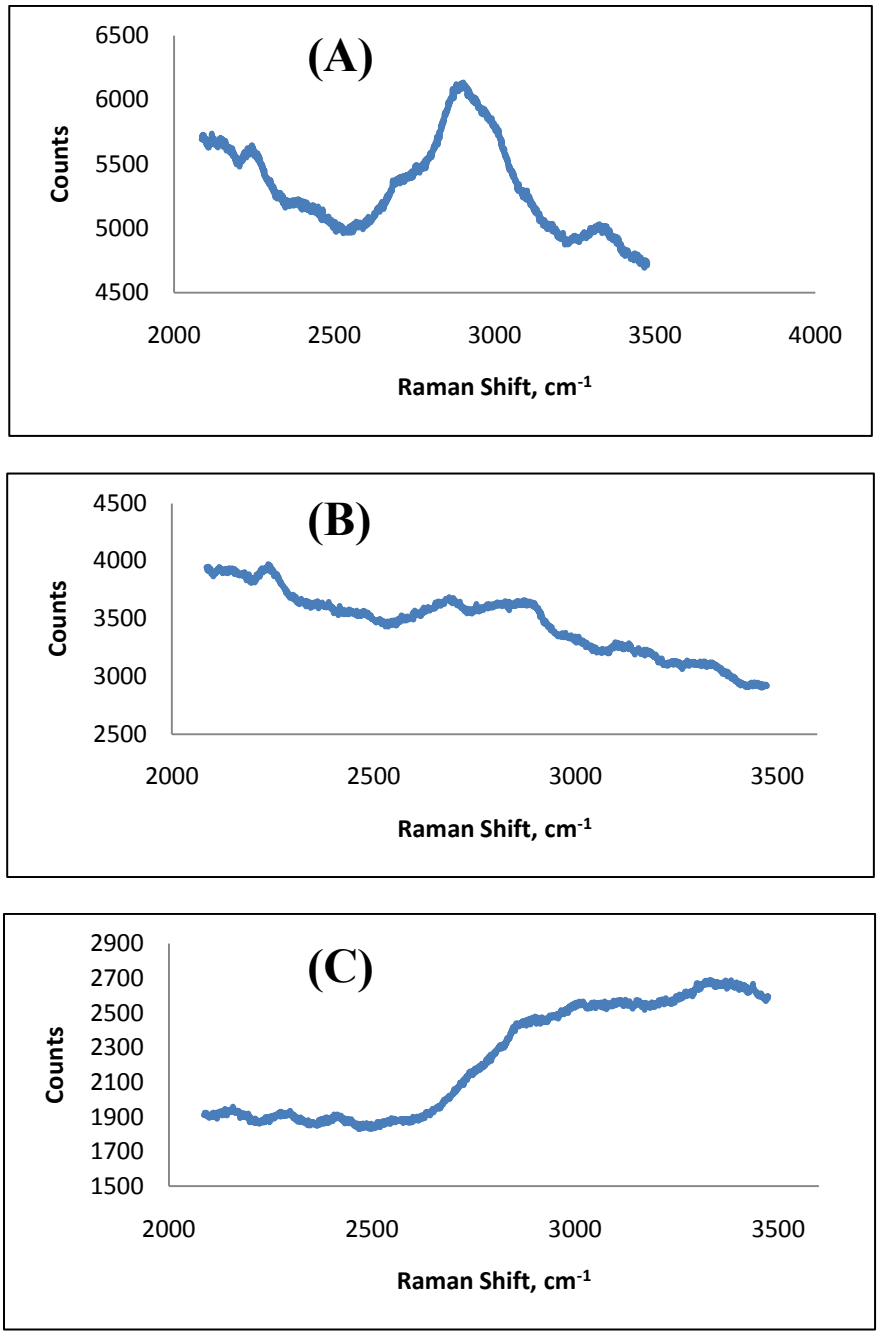


**Figure 4.3:** CARS signal for hexadecane sample. (A) Broad CARS signal for $CH_2$ symmetric stretch at ~2800 – 3000 $cm^{-1}$. (B) Spectrum obtained when Stokes beam is blocked. (C) Spectrum obtained when pump beam is blocked. All spectra were obtained with 118 mW pump power, 38 mW Stokes power, 50µm slit width for the monochromator, 1200 groove/mm grating and 10 s acquisition time.

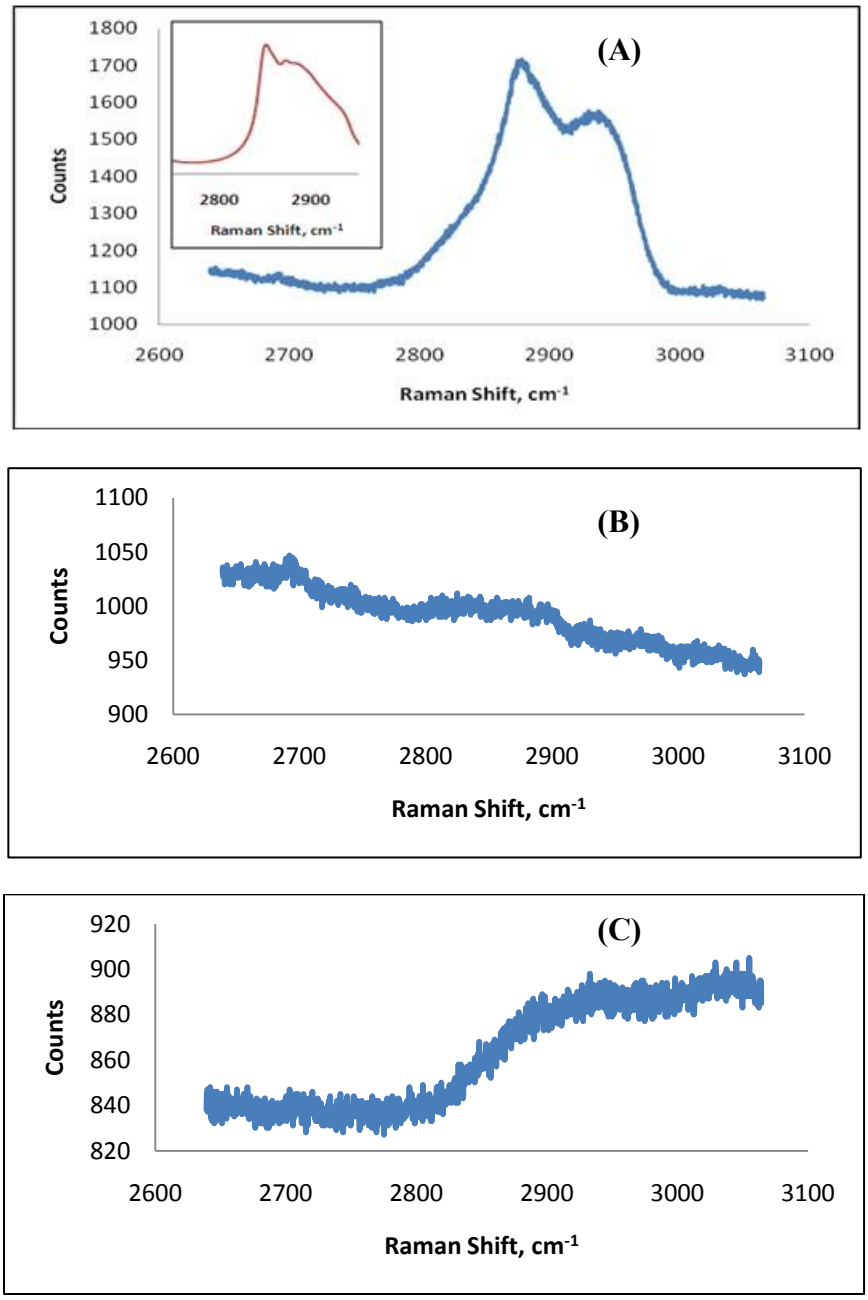


**Figure 4.4:** CARS signal for hexadecane sample after optimization of time and spatial overlap and better filtration of exciting beams. **(A)** Broad CARS signal for $CH_2$ symmetric stretch at ~2880 $cm^{-1}$. Inset shows the spontaneous Raman spectrum of hexadecane. **(B)** Spectrum obtained when Stokes beam is blocked. **(C)** Spectrum obtained when pump beam is blocked. All CARS spectra were obtained with 118 mW pump power, 38 mW Stokes power, 50µm slit width for the monochromator, 1200 groove/mm grating and 1s acquisition time. Raman spectrum obtained with Lambda Solutions Dimension-P2 Raman system, 785 nm laser, 200 mW and 1s integration time

# CHAPTER 5

## SUMMARY AND FUTURE WORK

This thesis aims to describe in detail the construction, optimization and testing of the CARS microscope set-up in the Allen Laboratory. The microscope is a broadband epi-CARS set-up where a narrow bandwidth pulse is used as the pump beam and a supercontinuum light source generated from a photonic crystal fiber is served as the Stokes beam. The two beams are spatially and temporally overlapped and focused tightly to the sample using an objective lens. The correct time overlap was set by measuring the path lengths of each beam as accurately as possible and adjusting the time delay stage to set the two path lengths equal. A nonlinear BBO crystal was used in setting the correct time overlap by observing the sum frequency signal generated at the zero-delay point. For the initial generation of a CARS signal, a forward CARS detection system was set-up using hexadecane as the sample and probe the $CH_2$ symmetric stretch at ~2845 $cm^{-1}$. The bandpass filter was taken out to increase the power for the pump beam. A broad CARS signal was generated at ~2850 – 2950 $cm^{-1}$ for the $CH_2$ symmetric stretch. Further optimization of the set-up and better filtering of the exciting beams improved the signal to noise ratio of the signal.

After detection of a forward generated CARS signal, the two beams are sent to the microscope and focused to the sample stage. The signal is then collected in the epi-direction by the same objective lens that is used to focus the exciting beams. The signal exits the side port of the microscope and directed towards the detection system. At present, this epi-detection set-up with the microscope is still being optimized for the generation of an epi-CARS signal. Figure 3.8 shows the signal collection set-up for epi-detection.

Table 5.1 compares various CARS microscopy set-ups from different research groups and this table suggests that even at lower power, CARS signal can be detected. The pump and Stokes power used for these set-ups are comparable and have lower power than the laser used for the system being described in this thesis, which is ~17 mW for the pump beam (with bandpass filter) and 38 mW for the Stokes beam. The broadband CARS microscope set-up of Kano et al.[40] and Murugkar et al.[47] have similar features to the CARS microscope being built as a photonic crystal fiber is used to generate the supercontinuum for the Stokes beam. The pump and Stokes power (13-15 mW pump beam and 0.5 – 3 mW Stokes beam) are also comparable to the pump and Stokes power (17 mW for the pump beam and 38 mW for the Stokes beam) used in this set-up. Their set-up however is for forward detection of CARS signal which is stronger and highly directional than an epi-CARS signal. Efficient collection of signal is needed to gather the CARS signal in the epi-direction. At present, efficient collection of signal is being done through thorough optimization of the set-up and proper alignment to be able to obtain an epi-CARS signal with a good spectral resolution and high signal to noise ratio.

The future work with the CARS set-up includes the investigation of dimethyl sulfoxide (DMSO) and giant unilammellar lipid vesicles as systems of study to demonstrate the limitations and resolution of the instrument. DMSO is an aprotic compound that possesses both a hydrophilic sulfoxide moiety and a hydrophobic component. The dual solubility of DMSO is largely responsible for its ability to penetrate biological membranes, and because of this ability it can be used for drug delivery across membranes.[48] CARS microscopy can be employed to study the penetration of DMSO across lipid membranes. The signal at 667 $cm^{-1}$ of DMSO for the C-S symmetric stretch can be probed using CARS microscopy. Figure 5.1 shows a Raman spectrum of DMSO with two isolated peaks at 667 $cm^{-1}$ and 698 $cm^{-1}$ for the C-S symmetric and asymmetric stretch respectively. By focusing the exciting beams inside and outside the lipid vesicles, the intensity of the DMSO signal can be compared overtime to determine the penetration of DMSO inside the vesicle. Also, by doing sample scanning and obtaining a spectrum point by point in a raster scan pattern, a sample image can be reconstructed by mapping the signal peaks of the $CH_2$ symmetric stretch (2840$cm^{-1}$) from the lipid membrane and the C-S symmetric stretch (667 $cm^{-1}$) of DMSO. In this way, the distribution and penetration of DMSO inside the lipid membrane can be clearly seen.

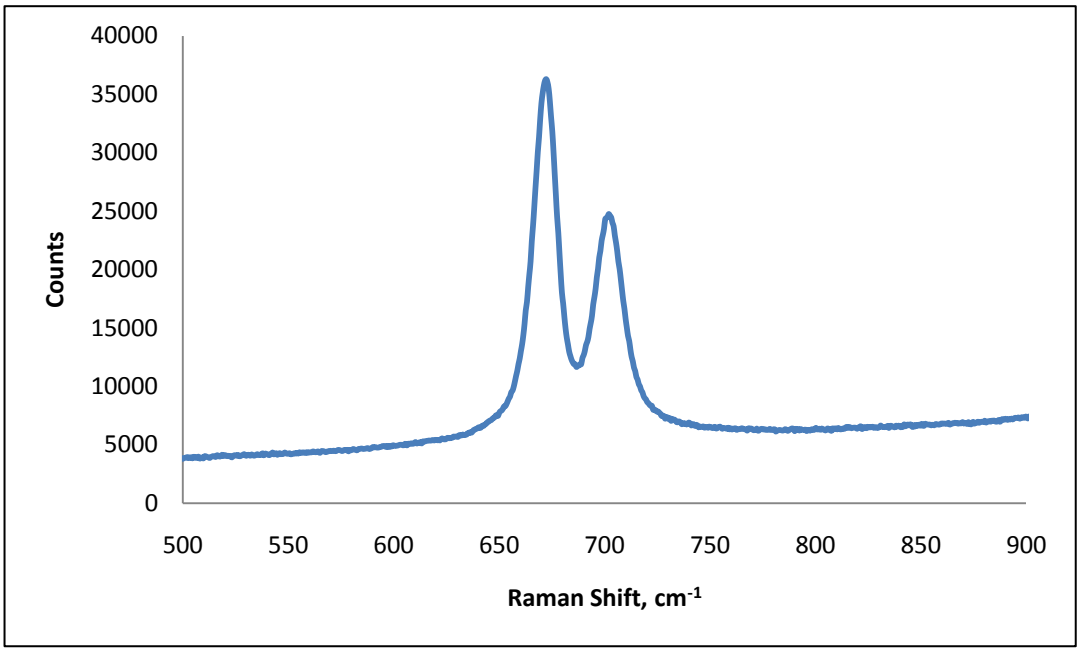


**Figure 5.1:** Raman Spectrum of DMSO. Laser: 532 nm, laser power: 200 mw, acquisition time: ~30s.

**Table 5.1: Comparison of CARS set-ups from different research groups**

| | Cheng (2008)[5,46] | Xie (1999)[18] | Xie (2001)[20] | Xie (2002)[47] |
|---|---|---|---|---|
| **CARS detection set-up** | Forward and Epi-CARS detection | Forward CARS detection | Forward and Epi-CARS detection | Laser scanning forward and Epi-CARS detection |
| **Laser** | Two synchronized Ti:Sapphire oscillators Coherent Inc, Mira 900) with 2.5 ps pulse trains | Two fs pulse trains generated from a Ti:Sapphire regenerative amplifier (Coherent Rega) Repetition rate: 250KHz | OPA pumped by a regeneratively amplified Ti:sapphire laser system Repetition rate: 250 kHz was | Two synchronized Ti:Sapphire oscillators (Tsunami, Spectra-Physics) with 5 ps pulse trains |
| **Laser power (at the sample)** | Pump: 3.0 mW Stokes: 1.4 mW | 120uw at 855nm and 50uw at 1.155um | Pump: 50 mW Stokes: 25 mW | Pump: 20 mW Stokes: 10 mW |
| **Microscope** | Confocal microscope (Olympus FV300/IX70) Water immersion objective with 1.2NA | Optical microscope Oil immersion objective (Nikon Plan Apo 60x, NA 1.4) | Inverted optical microscope (Nikon TE 300) Oil-immersion objective lens (Nikon Plan Apo, 60x, NA 1.4) | Confocal microscope: (Olympus FV300/IX70) Water objective lens with a NA 1.2 (UPLANAPO, 60X,Olympus) |
| **Signal collection and detection** | **Signal collection:** F-CARS: air condenser E-CARS: water immersion objective **Detector:** Photomultipliers (Hamamatsu R3896 and H7422-40) | **Signal collection:** Oil-immersion objective lens | **Signal Collection:** Objective lens **Detector:** Avalanche photodiodes (SPCM-APD 200, EG&G Canada | **Signal Collection:** **F-CARS:** air condenser lens (NA 0.55) **E-CARS**: water objective lens **Detector:** PMT (Hamamatsu, R3896) |
| **Schematic** | Refer to Figure 5.2A | | Refer to Figure 5.2B | Refer to Figure 5.2C |

*Continued*

**Table 5.1:** ***Continued***

| | Xie (2002)[27] | Evans, Xie (2005)[8] | Xie (2007)[48] | Muller (2002 and 2009)[28,49] |
|---|---|---|---|---|
| **CARS detection set-up** | Broadband Forward CARS detection | Video-rate Epi-CARS detection | Forward CARS detection | Broadband Forward CARS detection |
| **Laser** | Ps pump and fs Stokes beams from two Ti:sapphire lasers (Spectra-Physics, Tsunami) pumped by a 532 nm cw laser (Spectra-Physics, 10 W Millennia)<br>Repetition rate: 400 KHz | Mode-locked ps Nd:vanadate laser with 10-W output power (High-Q Laser)<br>Repetition rate:76 MHz<br>10% of output power is used to pump an OPO (Levante, APE) | Mode-locked Nd:YVO4 oscillator (High Q Laser, PicoTrain) which delivers ~6 ps pulse train at 1064 and 532 nm with a repetition rate of 80 MHz<br>The 532 nm light is used to pump an OPO (APE GmbH, Levante Emerald) | 10 ps pump pulse and 80 fs Stokes pulse from two mode-locked Ti:Sapphire lasers<br>Repetition rate: 80 MHz |
| **Laser power (at the sample)** | Pump: 0.6 – 1.2 mw<br>Stokes: 0.3 – 0.6 mw | Pump and Stokes beam: ~ 50mW | ~ 10-100 mW | Pump: ~20 mW<br>Stokes: ~3 mW |
| **Microscope** | Inverted microscope (Nikon, TE300)<br>Water objective (Olympus, UPIANAPO, 60X, NA 1.2) | Modified microscope for real time imaging (Vivascope)<br>Water objective: 1.2 NA, 60x (UPlanApo, Olympus) | Laser scanning microscope (Olympus, FV300-IX71)<br>Water immersion objective (NA 1.2, 60x, Olympus UPlanSApo) | Oil immersion objective 1.25 NA/63x |
| **Signal collection and detection** | **Signal Collection:**<br>F-CARS: Oil objective lens (Nikon, PLANAPO, 60X, NA1.4)<br>**Detector:**<br>*CARS image:*<br>Avalanche photodiode (EG&G, Model SPCM-AQR-14)<br>*CARS spectrum:*<br>Spectrograph (Acton Spectrapro-150) and CCD detector (Princeton Instruments) | **Signal Collection:**<br>E-CARS: Water objective: 1.2 NA, 60x (UPlanApo, Olympus)<br>**Detector:** Photomultiplier tube (R3896, Hamamatsu) | **Signal Collection**:<br>Condenser<br>**Detector:**<br>Photomultiplier tube (Hamamatsu, R9876) | **Signal Collection:**<br>Oil immersion objective (1.25 NA, 100x)<br>40x, 0.6 NA (Zeiss)<br>**Detector**<br>Spectrograph (Oriel MS257) with an Andor CCD camera ( V420-OE) |
| **Schematic** | Refer to Figure 5.3D | Refer to Figure 5.3E | Refer to Figure 5.3F | Refer to Figure 5.3G |

*Continued*

**Table 5.1:** ***Continued***

| | Moger (2008)[50] | Cicerone (2004)[51] | Kano and Hamaguchi (2005)[11] | Murugkar (2007)[52] |
|---|---|---|---|---|
| **CARS detection set-up** | Laser scanning forward and Epi-CARS detection | Broadband Forward CARS detection | Multiplex Forward CARS using supercontinuum generated from PCF | Multiplex Forward CARS using supercontinuum generated from PCF |
| **Laser** | Nd:Vanadium picosecond oscillator (High-Q Laser Production GmbH) is used to pump an OPO (Levante Emerald, APE).<br>The pump laser generates a 6 ps, 76 MHz pulse train of 532 nm laser light (10W output power) | Ti:sapphire oscillator (Coherent Mira 900F)7 pumped by a 6-W Nd:YVO4 laser (Coherent Verdi), producing 150-fs pulses at 785 nm<br>Repetition rate: 76 MHz | Mode-locked 100 fs Ti:sapphire laser (Coherent, Vitesse-800).<br>Repetition rate:80 MHz | Ti:sapphire laser producing ~ 65 fs pulses<br>Repetition rate: 80 MHz<br>Split into two arms for pump and Stokes beam<br>300mW input power to PCF |
| **Laser power (at the sample)** | Combined laser power of pump and Stokes beam: 100mW | Pump beam: 13 mW<br>Stokes beam: 10mW | Pump: 13 mW<br>Stokes: 3 mW | Pump beam: ~ 15 mW<br>Stokes beam: ~ 0.5 mW |
| **Microscope** | Modified inverted microscope and confocal laser scanner (IX71 and FV300, Olympus UK)<br>Water immersion objective, 60X, 1.2 NA (UPlanS Apo, Olympus UK) | 0.8-N.A. microscope objective | Inverted microscope (Nikon, TE2000-S)<br>40× and 0.9 NA microscope objective | Oil immersion objective (1.3 NA, 40x, Zeiss Plan Neofluar) |
| **Signal collection and detection** | **Signal Collection:**<br>F-CARS: Air condenser (NA=0.55)<br>E-CARS: Water immersion objective, 60X, 1.2 NA (UPlanS Apo, Olympus UK)<br>**Detector:**<br>Forward and Epi-CARS: Photomultiplier tube (R3896, Hamamatsu) | **Signal Collection:**<br>0.5 N.A. objective<br>**Detector:**<br>Spectrograph (Chromex 250IS) with a CCD camera (Andor) | **Signal Collection:**<br>F-CARS: 40×, 0.6-NA microscope objective<br>**Detector:**<br>Monochromator (Acton, SpectraPro-300i)<br>Photomultiplier tube (Hamamatsu, H957-08) | **Signal Collection:**<br>F-CARS: Water immersion objective (40x, 0.8 NA, Olympus)<br>**Detector:** Photomultiplier tube |
| **Schematic** | Refer to Figure 5.4H | Refer to Figure 5.4I | Refer to Figure 5.4J | Refer to Figure 5.4K |

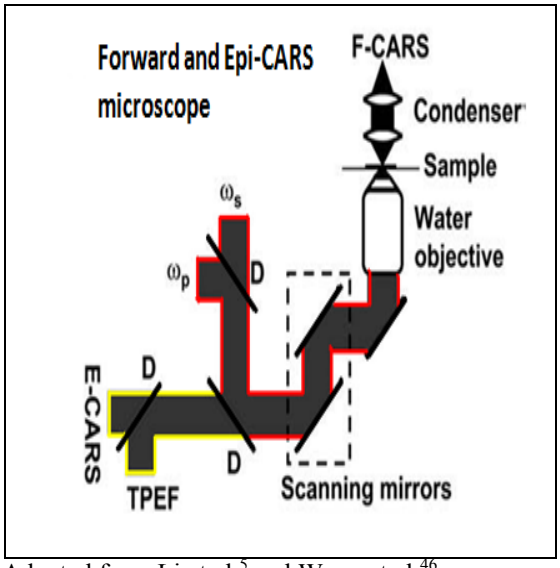


Adapted from Li et al.[5] and Wang et al.[46]

(A)

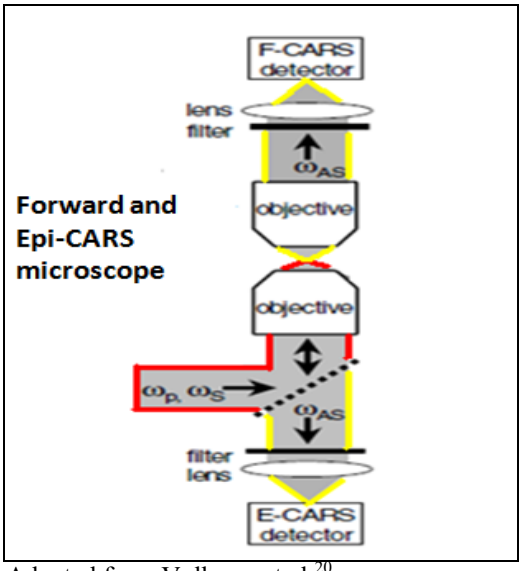


Adapted from Volkmer et al.[20]

(B)

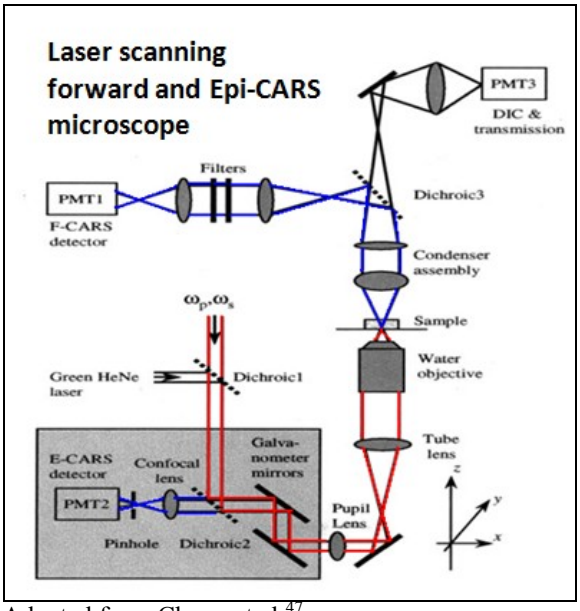


Adapted from Cheng et al.[47]

(C)

**Figure 5.2** Schematic diagram of various CARS set-up from Table 5.1.

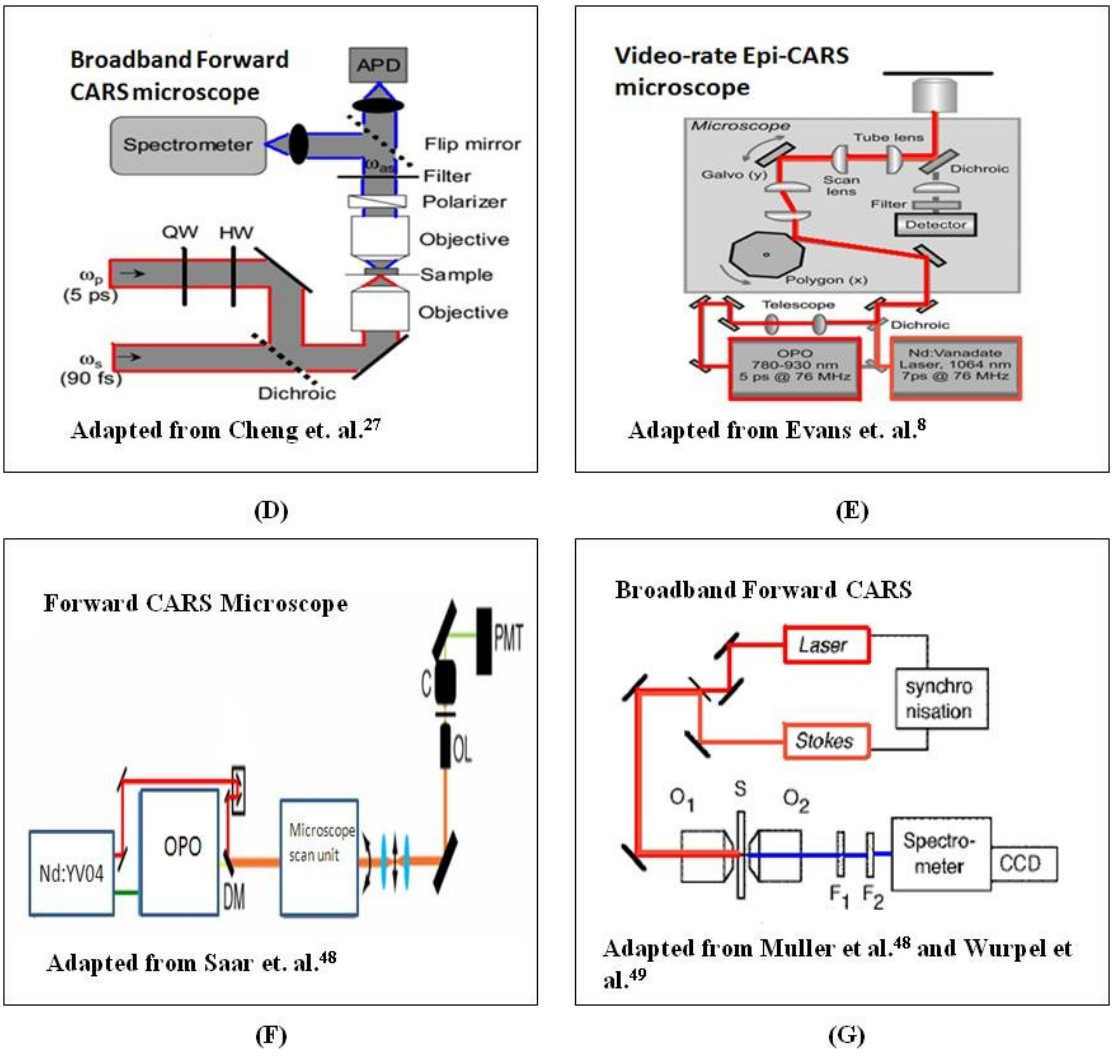


**Figure 5.3:** Schematic diagram of various CARS set-up from Table 5.1.

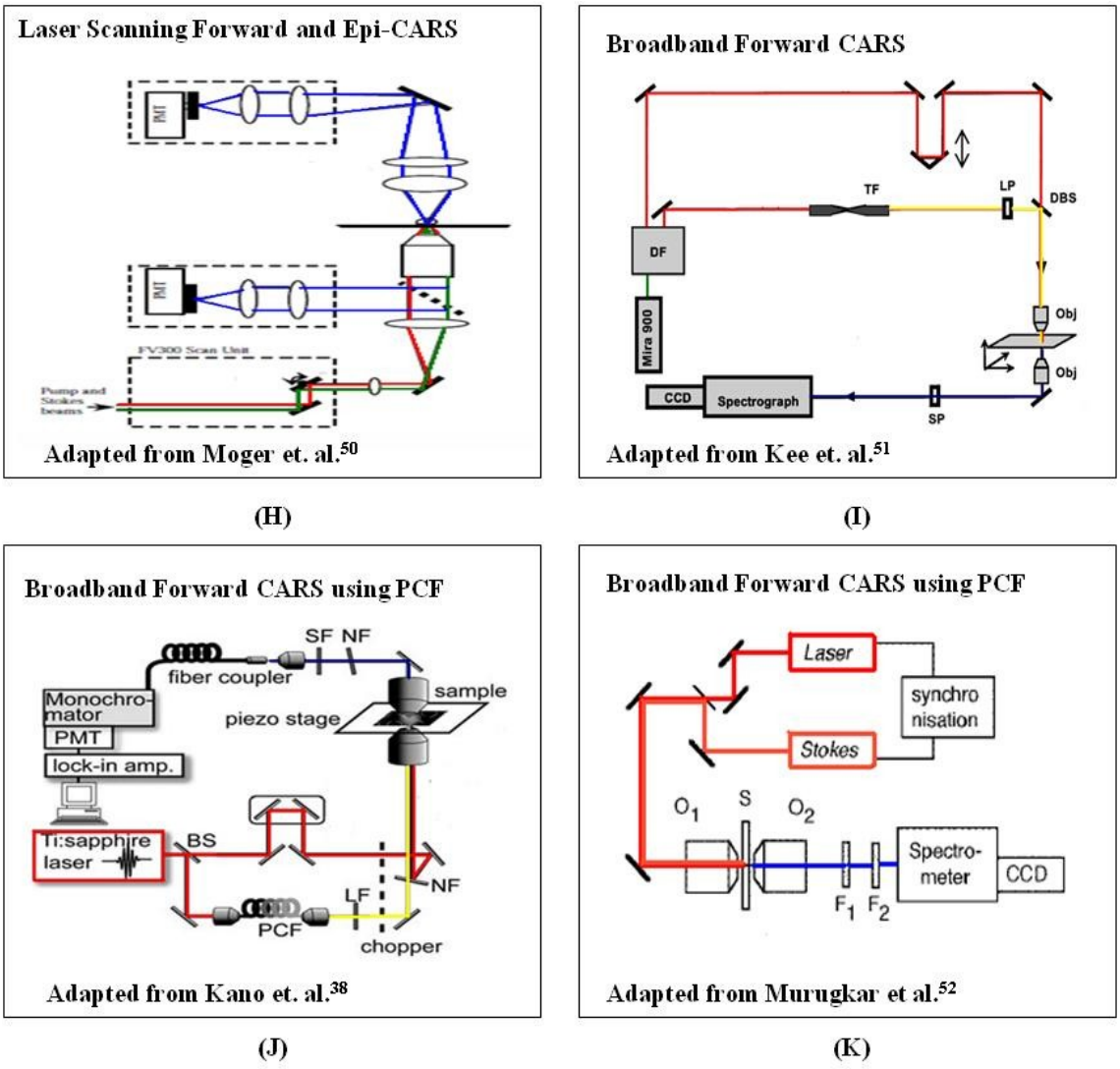


**Figure 5.4:** Schematic diagram of various CARS set-up from Table 5.1.

## REFERENCES


(1) Vanderkooi. Vibrational Spectroscopy, 2006.

(2) Rodriguez, L. G.; Lockett, S. J.; Holtom, G. R. *Coherent anti-stokes Raman scattering microscopy: A biological review.* Cytometry Part A. **2006**, 69A, 779-791.

(3) Muller, M.; Zumbusch, A. *Coherent anti-stokes Raman scattering microscopy.* Chemphyschem. **2007**, 8, 2156-2170.

(4) Potma, E. O.; Xie, X. S. *CARS Microscopy*. In Optics and Photonics News, 2004; pp 40-45.

(5) Li, L.; Cheng, J. X. *Label-free coherent anti-stokes Raman scattering imaging of coexisting lipid domains in single bilayers.* Journal of Physical Chemistry B. **2008**, 112, 1576-1579.

(6) Cheng, J. X.; Pautot, S.; Weitz, D. A.; Xie, X. S. *Ordering of water molecules between phospholipid bilayers visualized by coherent anti-Stokes Raman scattering microscopy.* Proceedings of the National Academy of Sciences of the United States of America. **2003**, 100, 9826-9830.

(7) Evans, C. L.; Xie, X. S. *Coherent Anti-Stokes Raman Scattering Microscopy: Chemical Imaging for Biology and Medicine.* Annual Review of Analytical Chemistry. **2008**, 1, 883-909.

(8) Evans, C. L.; Potma, E. O.; Puoris'haag, M.; Cote, D.; Lin, C. P.; Xie, X. S. *Chemical imaging of tissue in vivo with video-rate coherent anti-Stokes Raman scattering microscopy.* Proceedings of the National Academy of Sciences of the United States of America. **2005**, 102, 16807-16812.

(9) Evans, C. L.; Xu, X. Y.; Kesari, S.; Xie, X. S.; Wong, S. T. C.; Young, G. S. *Chemically-selective imaging of brain structures with CARS microscopy.* Optics Express. **2007**, 15, 12076-12087.

(10) Pudney, P. D. A.; Melot, M.; Caspers, P. J.; van der Pol, A.; Puppels, G. J. *An in vivo confocal Raman study of the delivery of trans-retinol to the skin.* Applied Spectroscopy. **2007**, 61, 804-811.

(11) Maker, P. D.; Terhune, R. W. *Study Of Optical Effects Due To An Induced Polarization Third Order In Electric Field Strength.* Physical Review. **1965**, 137, A801-A818.

(12) Lasch, P.; J., K. *Biomedical Vibrational Spectroscopy*; Wiley-Interscience, 2008.

(13) Coherent anti-Stokes Raman Scattering http://en.wikipedia.org/wiki/Coherent_anti-Stokes_Raman_spectroscopy.

(14) Begley, R. F.; Harvey, A. B.; Byer, R. L. *Coherent Anti-Stokes Raman-Spectroscopy.* Applied Physics Letters. **1974**, 25, 387-390.

(15) Potma, E. O.; Xie, X. S. *Theory of Spontaneous and Coherent Raman Scattering*. In *Handbook of Biomedical Nonlinear Optical Microscopy*; Masters, B. R., So, P. T. C., Eds.; Oxford University Press: New York, New York 2008; pp 164-186.

(16) Cheng, J. X.; Xie, X. S. *Coherent anti-Stokes Raman scattering microscopy: Instrumentation, theory, and applications.* Journal of Physical Chemistry B. **2004**, 108, 827-840.

(17) Duncan, M. D.; Reintjes, J.; Manuccia, T. J. *Scanning Coherent Anti-Stokes Raman Microscope.* Optics Letters. **1982**, 7, 350-352.

(18) Zumbusch, A.; Holtom, G. R.; Xie, X. S. *Three-dimensional vibrational imaging by coherent anti-Stokes Raman scattering.* Physical Review Letters. **1999**, 82, 4142-4145.

(19) Cheng, J. X.; Volkmer, A.; Book, L. D.; Xie, X. S. *An epi-detected coherent anti-stokes raman scattering (E-CARS) microscope with high spectral resolution and high sensitivity.* Journal of Physical Chemistry B. **2001**, 105, 1277-1280.

(20) Volkmer, A.; Cheng, J. X.; Xie, X. S. *Vibrational imaging with high sensitivity via epidetected coherent anti-Stokes Raman scattering microscopy.* Physical Review Letters. **2001**, 87.

(21) Ingle, J. D.; Crouch, S. R. *Spectrochemical Analysis*; Prentice Hall: New Jersey, 1988.

(22) Boyd, R. W. *Nonlinear Optics* 2nd ed.; Academic Press, 2003.

(23) Lambert, A. G.; Davies, P. B.; Neivandt, D. J. *Implementing the theory of sum frequency generation vibrational spectroscopy: A tutorial review.* Applied Spectroscopy Reviews. **2005**, 40, 103-145.

(24) Hudson, B.; Hetherington, W.; Cramer, S.; Chabay, I.; Klauminzer, G. K. *Resonance Enhanced Coherent Anti-Stokes Raman-Scattering.* Proceedings of the National Academy of Sciences of the United States of America. **1976**, 73, 3798-3802.

(25) Tolles, W. M.; Nibler, J. W.; McDonald, J. R.; Harvey, A. B. *Review Of Theory And Application Of Coherent Anti-Stokes Raman-Spectroscopy (CARS).* Applied Spectroscopy. **1977**, 31, 253-271.

(26) Muller, M.; Squier, J.; De Lange, C. A.; Brakenhoff, G. J. *CARS microscopy with folded BoxCARS phasematching.* Journal of Microscopy-Oxford. **2000**, 197, 150-158.

(27) Shirley, J. A.; Hall, R. J.; Eckbreth, A. C. *Folded BOXCARS For Rotational Raman Studies.* Optics Letters. **1980**, 5, 380-382.

(28) Cheng, J. X.; Volkmer, A.; Xie, X. S. *Theoretical and experimental characterization of coherent anti-Stokes Raman scattering microscopy.* Journal of the Optical Society of America B-Optical Physics. **2002**, 19, 1363-1375.

(29) Chen, J. X.; Volkmer, A.; Book, L. D.; Xie, X. S. *Multiplex coherent anti-stokes Raman scattering microspectroscopy and study of lipid vesicles.* Journal of Physical Chemistry B. **2002**, 106, 8493-8498.

(30) Muller, M.; Schins, J. M. *Imaging the thermodynamic state of lipid membranes with multiplex CARS microscopy.* Journal of Physical Chemistry B. **2002**, 106, 3715-3723.

(31) Shen, Y. R. *The Principles of Nonlinear Optics*; John Wiley and Sons Inc.: New York, 1984.

(32) Voroshilov, A.; Otto, C.; Greve, J. *On the coherent vibrational phase in polarization sensitive resonance CARS spectroscopy of copper tetraphenylporphyrin.* Journal of Chemical Physics. **1997**, 106, 2589-2598.

(33) Wurpel, G. W. H.; Schins, J. M.; Muller, M. *Chemical specificity in 3D imaging with multiplex CARS microscopy.* Biophysical Journal. **2003**, 84, 48A-48A.

(34) *Coherent Anti-Stokes Raman Scattering Microscpectrometer: Application 36.* Newport Corporation Technology and Application Center.

(35) Broadband Optical Isolator. Newport Corporation. www.newport.com.

(36) *Variable Attenuator for Lasers: Application 26.* Newport Corporation Technology and Application Center

(37) *Supercontinuum Generation in SCG-800 Photonic Crystal: Application 28*. Newport Corporation Technology and Application Center.

(38) Bjarklev, A.; Broeng, J.; Bjarklev, A. *Photonic Crystal Fiber*; Kluwer Academic Publishers, 2003.

(39) Supercontinuum Generation. NKT Photonics. http://www.nktphotonics.com/side5412-cid-7858.html.

(40) Kano, H.; Hamaguchi, H. *Near-infrared coherent anti-Stokes Raman scattering microscopy using supercontinuum generated from a photonic crystal fiber.* Applied Physics B-Lasers and Optics. **2005**, 80, 243-246.

(41) Gaubert, N. *Modifying An Inverted Laboratory Microscope For Raman Microscopy.* Master Thesis, The Ohio State University, 2006.

(42) Shamrock 303i. Andor Technology. https://www.andor.com/pdfs/specs/s303SS.pdf. .

(43) Supercontinuum Generation in Photonic Crystal Fibers. NKT Photonics Application Note. Version 2.0. http://www.nktphotonics.com/files/files/Application_note_-_Supercontinuum%20-%20General.pdf, 2009.

(44) Users Guide To Shamrock sr-303i. Andor Technology, Version 2.5, 2005.

(45) Filter Spectra at Non-normal Angles of Incidence. Semrock, Inc. http://www.semrock.com/TechnicalInformation/TN_Filter_spectra_at_nonnormal_angles_of_incidence/.

(46) McCreery, R. L. *Raman Spectroscopy for Chemical Analysis*; John Wiley and Sons: New York, 2000.

(47) Murugkar, S.; Brideau, C.; Ridsdale, A.; Naji, M.; Stys, P. K.; Anis, H. *Coherent anti-Stokes Raman scattering microscopy using photonic crystal fiber with two closely lying zero dispersion wavelengths.* Optics Express. **2007**, 15, 14028-14037.

(48) Tarshis, B. *DMSO: The True Story of a Remarkable Pain-Killing Drug*; William Morrow and Company, Inc., 1981.